NASA Technical Paper 1325

A Theoretical Investigation of Noise Reduction Through the Cylindrical Fuselage of a Twin-Engine, Propeller-Driven Aircraft

Rama B. Bhat and John S. Mixson

DECEMBER 1978

NASA

NASA Technical Paper 1325

A Theoretical Investigation of Noise Reduction Through the Cylindrical Fuselage of a Twin-Engine, Propeller-Driven Aircraft

Rama B. Bhat and John S. Mixson
Langley Research Center
Hampton, Virginia

SUMMARY

Interior noise in the fuselage of a twin-engine, propeller-driven aircraft with two propellers rotating in opposite directions is studied analytically. The fuselage is modeled as a stiffened cylindrical shell with simply supported ends, and the effect of stringers and frames is averaged over the shell surface. An approximate mathematical model of the propeller noise excitation is formulated which includes some of the propeller noise characteristics such as sweeping pressure waves around the sidewalls due to propeller rotation and the localized nature of the excitation with the highest levels near the propeller plane. Results are presented in the form of noise reduction, which is the difference between the levels of external and interior noise. The influence of propeller noise characteristics on the noise reduction is studied. The results indicate that the sweep velocity of the excitation around the fuselage sidewalls is critical to noise reduction.

INTRODUCTION

One of the main sources of interior noise in propeller-driven aircraft is the propeller noise excitation. A main path by which noise is transmitted to the interior is through the fuselage structure. The present paper is devoted to the study of the noise reduction provided by the fuselage structure when subjected to propeller noise excitation and the influence of propeller noise characteristics on the noise reduction.

Some information is available on the nature of the propeller noise and its near field behavior (refs. 1 to 7) which reveals a few characteristics of propeller noise such as (1) the pressure field rotating with the blades causing a sweeping action around the sidewalls of the fuselage, (2) the localized nature of the noise field on the fuselage surface with highest levels near the propeller plane, and (3) the noise spectrum dominated by propeller harmonics. References 8, 9, and 10 analyze interior noise in fuselages using statistical energy analysis and deterministic analyses for exterior noise pressure inputs such as turbulent boundary layers, jet noise, or plain acoustic waves. Interior noise in propeller-driven light aircraft with flat fuselage sidewalls has been studied experimentally (ref. 11), and analytically considering uniform pressure to represent propeller noise input on the sidewalls (ref. 12).

The present investigation extends previous analyses by employing a more realistic representation of propeller excitation pressures and complements the studies discussed in reference 12 with regard to fuselage geometry by considering cylindrical fuselages. An approximate mathematical model has been developed, using information available in the references, for the propeller noise excitation which includes some of the propeller noise characteristics. Twin-engine aircraft with propellers rotating in opposite directions are considered. The noise fields from the propellers on either side of the fuselage are assumed to be symmetrical about the central vertical plane of the fuselage. The objective

\

of the present investigation is to study the quantitative influence of the pro-
peller noise characteristics on the noise reduction through the fuselage side-
walls. Two sizes of fuselage structure are studied, one representative of a
large passenger aircraft fuselage and the other corresponding to that of a light
aircraft fuselage.

The overall development of the analysis in this study closely follows that
in reference 10. The fuselage is modeled as a cylindrical shell stiffened by
stringers and ring frames and having simply supported ends. The effects of
stiffeners are averaged over the fuselage surface. The analysis for the interior
noise in the fuselage is carried out using the approximate model of propeller
noise input on the fuselage structure and the normal mode approach to determine
the response of the fuselage and the resulting pressure fluctuations in the
interior acoustic field. The frequency range considered is from 0 to 500 Hz and
includes the blade passage frequency and the first few harmonics, which are the
dominant sources of propeller noise. The noise reduction through the fuselage
sidewalls is the difference between the excitation noise level on the fuselage
surface and the space-averaged interior noise level within the fuselage. Results
showing the influence of propeller noise characteristics on noise reduction are
presented.

SYMBOLS

The units used for physical quantities defined in this paper are given in
the International System (SI) of units.

A_r, A_s cross-sectional areas of ring frame and stringer, respectively, m^2

a_1, a_2, b_1, b_2 distances defining the fuselage surface area subjected to pro-
peller noise excitation, shown in figure 1, m

C_1, C_2, C_3, C_4 constants appearing in equation (B2)

C_{mni} modal constant defined in equation (B11)

c speed of sound in air, m/sec

E modulus of elasticity of fuselage material, Pa

E_r, E_s moduli of elasticity of ring frame and stringer materials,
respectively, Pa

F_{mni} generalized force for (mni) mode

f frequency, Hz

f_r reference frequency, Hz

G_r, G_s shear moduli of ring frame and stringer materials, respectively, Pa

H frequency response defined in equation (6)

2

h	thickness of fuselage material, m
I_{mni}	integrals defined in equations (11), (12), and (13)
I_n	modified Bessel function of first kind and of nth order
I_r, I_s	moments of inertia for ring frame and stringer, respectively
J_n	Bessel function of first kind and nth order
J_r, J_s	torsional constants for ring frame and stringer, respectively
k	wave number ω/c defined in equation (B3)
L	length of fuselage, m
L_{rs}	differential operators in equation (A1), $r,s = 1, 2, 3$
l_r, l_s	ring frame and stringer spacings, respectively, m
M_{mni}	generalized mass of (mni) mode
M_x	moment resultant in x-direction
m, ξ	number of half waves along cylinder axis
N_x	stress resultant in x-direction
n, η	number of full waves around cylinder circumference
P	pressure amplitude of excitation pressure, Pa
p	interior noise pressure, Pa
P_e	excitation pressure, Pa
Q_{ac}	dynamic magnification factor for acoustic modes
Q_{mni}	dynamic magnification factor for (mni) structural mode
q_{mni}	generalized coordinate of (mni) structural mode
R	radius of fuselage, m
r	radial coordinate of fuselage, m
$\hat{r}$	dimensionless radial coordinate r/R
s	number of radial acoustic waves
t	time, sec

U_{mni}	mode functions for fuselage displacements in x-direction
u	fuselage displacement in x-direction, m
u_1, u_2	fuselage displacement amplitudes in x-direction, m
V	sweep velocity of exciting pressure waves, m/sec
V_{mni}	mode functions for fuselage displacements in y-direction
v	fuselage displacement in y-direction, m
v_1, v_2	fuselage displacement amplitudes in y-direction, m
W_{mni}	mode functions for fuselage displacements in z-direction
w	radial displacement of fuselage, m
w_a	radial displacement of air particle in fuselage interior, m
x	coordinate in longitudinal direction of fuselage, m
y	coordinate in circumferential direction of fuselage, m
z	coordinate in radial direction of fuselage, m
z_r, z_s	eccentricities of ring frame and stringer centroids from fuselage skin middle plane, m
α	parameter defined in equation (B3)
γ_{mni}	quantity defined in equation (B17)
$\dot{\theta}$	phase angle of frequency response of fuselage displacement, rad
μ	Poisson's ratio for material of fuselage
ρ	density of fuselage skin material, kg/m^3
ρ_a	average density of skin-stringer fuselage structure, kg/m^3
ρ_o	density of air, kg/m^3
ρ_r, ρ_s	densities of ring frame and stringer materials, respectively, kg/m^3
Φ_{mni}	mode functions of (mni) acoustic modes
ϕ	coordinate in circumferential direction for interior acoustic space y/R
ψ	quantity defined in equations (B4)

4

ω frequency, rad/sec

ω_{mn} structural modal frequencies, rad/sec

ω_{mns} acoustic modal frequencies, rad/sec

Subscripts:

i,j,m,n,r,s,η,ξ integers

Dots over symbols denote time derivatives.

Primes over symbols denote derivatives with respect to spatial coordinates.

Bars over symbols denote amplitudes.

ANALYSIS

Since propeller noise is predominant near the blade passage frequency and the first few harmonics, which lie in the low-frequency range, a fuselage model that is simple but suitable in the low-frequency range is required. Such a model is available in reference 13 in which the effect of stringers and ring frames are averaged over the fuselage surface. Shown in figure 1(a) is a fuselage structure idealized as a simple cylindrical shell with reinforcing stringers and ring frames. The fuselage is excited by propeller noise excitation, and the resulting vibrations of the fuselage structure excite the interior air space causing interior noise. The displacement response of the fuselage walls is calculated using a normal mode approach. The interior noise in the fuselage is obtained by equating the displacement of the fuselage wall to that of the air particle near the wall. This plan of development follows reference 10 closely.

The following discussion gives the main features of the analysis. Details of the derivation of the forced-response equations for the fuselage structure are given in appendix A, and details of the interior noise derivations are given in appendix B.

Displacement Response of Fuselage Structure

The equation of motion for the (mni) mode of the fuselage structure is (see eq. (A13))

$$\ddot{q}_{mni}(t) + \frac{\omega_{mn}}{Q_{mni}} \dot{q}_{mni}(t) + \omega_{mn}^2 q_{mni}(t) = \frac{F_{mni}(t)}{M_{mni}} \tag{1}$$

where q_{mni} represents the generalized coordinates and ω_{mn} represents the natural frequencies of the fuselage structure. The subscripts (mni) specify

the resonant deflection shapes of the cylindrical shell where $m = 1, 2, 3, \ldots$ is the number of elastic half waves along the cylinder axis, $n = 1, 2, 3, \ldots$ is the number of elastic full waves around the cylinder circumference, and $i = 1, 2$ indicates the orthogonal solutions for mode shapes to specify the complete response since there is no preferred location of the origin of the y-axis. The first few modes are illustrated in figure 2. The dynamic magnification factors at resonance are denoted by Q_{mni}. The term M_{mni} is the generalized mass of the (mni) structural mode. (See eq. (A11).) The term F_{mni} is the generalized force of the (mni) structural mode given as

$$F_{mni}(t) = \iint P_e(x,y,t)\left[W_{mni}(x,y)dx\ dy\right] \tag{2}$$

where $P_e(x,y,t)$ is the external pressure loading on the fuselage surface and $W_{mni}(x,y)$ denotes the (mni) structural mode function. The complete radial displacement response of the shell is obtained by summing up the response of all the normal modes of the shell (eq. (A7c)) as

$$w(x,y,t) = \sum_{mni} W_{mni}(x,y)q_{mni}(t) \tag{3}$$

Assuming that the generalized force is harmonic at frequency ω; that is

$$F_{mni}(t) = \bar{F}_{mni}e^{i\omega t} \tag{4}$$

the solution of equation (1) can be written as

$$q_{mni}(t) = \frac{H(\omega/\omega_{mn})}{\omega_{mn}^2 M_{mni}} \exp\left[-\theta(\omega/\omega_{mn})\right]\bar{F}_{mni}e^{i\omega t} \tag{5}$$

where

$$H(\omega/\omega_{mn}) = \left\{\left[1 - (\omega/\omega_{mn})^2\right]^2 + \frac{1}{Q_{mni}^2}(\omega/\omega_{mn})^2\right\}^{-1/2} \tag{6}$$

and

$$\theta(\omega/\omega_{mn}) = \tan^{-1}\left\{\frac{\omega/\omega_{mn}}{Q_{mni}\left[1 - (\omega/\omega_{mn})^2\right]}\right\} \tag{7}$$

6

Subsequently, the radial displacement of the shell is obtained by combining equation (5) and equation (3) as

$$w(x,y,t) = \sum_{mni} \frac{H(\omega/\omega_{mn})}{\omega_{mn}^2 M_{mni}} \exp\left[-\theta(\omega/\omega_{mn})\right] \bar{F}_{mni} W_{mni}(x,y) e^{i\omega t} \tag{8}$$

Propeller Noise Excitation

Previous studies on the nature of the propeller noise (refs. 1 to 7) indicate that:

1. The noise field generated by the propeller blades rotates with the propeller.

2. The propeller noise exciting the fuselage surface has the highest levels near the propeller plane.

3. The spectrum of the propeller noise is dominated by propeller harmonics.

By employing these characteristics of propeller noise excitation an approximate mathematical model is formulated.

In figure 1(b) the location of the propellers is shown relative to the fuselage. The propeller noise on the fuselage is illustrated by the hatched area around the fuselage. It is assumed that the propellers on either side of the fuselage are rotating in opposite directions and also that their noise fields incident on the fuselage sidewalls are symmetrical with respect to the fuselage vertical plane of symmetry. It is also assumed that the noise field is traveling around the fuselage with constant velocity V, as shown in figure 1(b), by the arc around the fuselage. This approximate representation of the propeller noise field is mathematically expressed, for a particular propeller harmonic, as

$$\left. \begin{aligned} p_e(x,y,t) &= P \exp\left[i\omega\left(t - \frac{y-b_1}{V}\right)\right] && \begin{pmatrix} a_1 \leqq x \leqq a_2 \\ b_1 \leqq y \leqq b_2 \end{pmatrix} \\[2em] p_e(x,y,t) &= P \exp\left[i\omega\left(t + \frac{y+b_1}{V}\right)\right] && \begin{pmatrix} a_1 \leqq x \leqq a_2 \\ -b_2 \leqq y \leqq -b_1 \end{pmatrix} \\[2em] p_e(x,y,t) &= 0 && \text{(elsewhere)} \end{aligned} \right\} \tag{9}$$

where ω is the frequency of the harmonic, P is the amplitude of the exciting pressure, V is the velocity of the pressure waves traveling around the fuselage due to the propeller rotation, and a_1,a_2,b_1,b_2 specify the fuselage surface area subjected to propeller noise excitation. (See figs. l(a) and l(b).) The sweep velocity V and the frequency ω can be related to the propeller parameters. In equations (9), $V = \infty$ corresponds to the case of uniform pressure loading on the fuselage surface.

Combining equations (9) and equation (2) and making use of equations (A8) and (A9), the generalized force for the (mni) mode is obtained as

$$F_{mni}(t) = \bar{F}_{mni}e^{i\omega t} = Pe^{i\omega t}(I_{mni}) \tag{10}$$

The integrals I_{mni} in equation (10) are evaluated to obtain

$$I_{mn1} = 0 \tag{11}$$

due to the symmetry of the forcing pressure field about the vertical plane of symmetry of the fuselage, and

$$I_{mn2} = \frac{L}{m\pi}\left[\cos\ (m\pi a_1/L)\ -\ \cos\ (m\pi a_2/L)\right]$$

$$\times\left(\left\{\frac{\sin\left[\dfrac{nb_2}{R} + \dfrac{\omega}{V}(b_2 - b_1)\right] - \sin\dfrac{nb_1}{R}}{\dfrac{n}{R} + \dfrac{\omega}{V}} + \frac{\sin\left[\dfrac{nb_2}{R} - \dfrac{\omega}{V}(b_2 - b_1)\right] - \sin\dfrac{nb_1}{R}}{\dfrac{n}{R} - \dfrac{\omega}{V}}\right\}\right.$$

$$\left.+ i\left\{\frac{\cos\left[\dfrac{nb_2}{R} + \dfrac{\omega}{V}(b_2 - b_1)\right] - \cos\dfrac{nb_1}{R}}{\dfrac{n}{R} + \dfrac{\omega}{V}} + \frac{\cos\dfrac{nb_1}{R} - \cos\left[\dfrac{nb_2}{R} - \dfrac{\omega}{V}(b_2 - b_1)\right]}{\dfrac{n}{R} - \dfrac{\omega}{V}}\right\}\right)$$

$$\tag{12}$$

when $n/R \neq \omega/V$ and

$$I_{mn2} = \frac{L}{m\pi}\Big[\cos\,(m\pi a_1/L) - \cos\,(m\pi a_2/L)\Big]$$

$$\times \left(\left\{\frac{\sin\left[\dfrac{nb_2}{R} + \dfrac{\omega}{V}(b_2 - b_1)\right] - \sin\dfrac{nb_1}{R}}{\dfrac{n}{R} + \dfrac{\omega}{V}} + (b_2 - b_1)\,\cos\dfrac{\omega b_1}{V}\right\}\right.$$

$$\left. + \, i\left\{\frac{\cos\left[\dfrac{nb_2}{R} + \dfrac{\omega}{V}(b_2 - b_1)\right] - \cos\dfrac{nb_1}{R}}{\dfrac{n}{R} + \dfrac{\omega}{V}} + (b_2 - b_1)\,\sin\dfrac{\omega b_1}{V}\right\}\right) \tag{13}$$

when $n/R = \omega/V$. In equation (13) when $n/R = \omega/V$, the sweep velocity V matches with the bending wave velocity around the fuselage $\omega R/n$ and hence corresponds to the case of coincidence. Substitution of the generalized force given in equation (10) into equation (8) yields the displacement response of the fuselage structure.

Interior Noise Analysis

The internal acoustic field, which is excited by the fuselage vibrations, is defined by the wave equation

$$\nabla^2 p = \frac{1}{c^2}\frac{\partial^2 p}{\partial t^2} \tag{14}$$

and the boundary conditions chosen for the ends and wall of the cylindrical section. To permit simplified analysis, open-end conditions are assumed; that is, the acoustic impedance, which is defined as the ratio of acoustic pressure to particle velocity, is taken as zero. While it is recognized that in an actual fuselage the ends have finite impedance, the use of the open-end conditions should have little effect on the calculated modal density of the sound field in the frequency range considered.

An expression for the interior noise pressure is obtained by assuming the boundary conditions at the wall to be such that the acoustic and the structural

9

analyses are coupled. The radial deflections of the shell are equated to the radial displacements of the air particles adjacent to the shell walls in the interior space. (See appendix B for detailed analysis.) The expressions for the space-averaged mean-square interior noise is given by (see eqs. (B16), (B18), and (B25))

$$\overline{p^2}(\omega) = \overline{P^2}\rho_o^2 R^2 \omega^4 \sum_{mni} \frac{\left|H(\omega/\omega_{mn})\right|^2}{M_{mni}^2 \omega_{mn}^4} \left\{\frac{\left|I_{mni}\right|^2 \gamma_{mni}}{\alpha^2 \left[J_n'(\alpha)\right]^2}\right\}$$

$$\times \left\{J_n^2(\alpha) - J_{n-1}(\alpha)\left[J_{n+1}(\alpha)\right]\right\} \tag{15}$$

In equation (15), $J_n'(\alpha) \rightarrow 0$ is the condition of acoustic resonance. The acoustic resonance frequencies are given by ω_{mns} (see eq. (B14)) where $m = 1, 2, 3, \ldots$ is the number of longitudinal half waves, $n = 1, 2, 3, \ldots$ is the number of circumferential full waves, and $s = 1, 2, 3, \ldots$ is the number of radial waves. Nodal patterns for a few acoustic modes are shown in figure 3. At resonance the interior noise is given by

$$\overline{p^2}(\omega) = \overline{P^2}\rho_o^2 R^2 \omega^4 \sum_{mni} \frac{\left|H(\omega/\omega_{mn})\right|^2}{M_{mni}^2 \omega_{mn}^4} \left\{\frac{\left|I_{mni}\right|^2 \gamma_{mni}\left(4Q_{ac}^2\right)}{k^4 R^4 \left[J_n''(\alpha_{ns})\right]^2}\right\}$$

$$\times \left\{J_n^2(\alpha) - J_{n-1}(\alpha)\left[J_{n+1}(\alpha)\right]\right\} \tag{16}$$

RESULTS

Results are presented for two fuselage structures whose dimensions are shown in table I. Fuselage 1 is representative of a large passenger-aircraft fuselage and fuselage 2 corresponds to a light-aircraft fuselage. The properties of the fuselage material and air in the fuselage interior are given in table II. The magnification factor for structural modes Q_{mni} is chosen as 50, which corresponds to 1 percent of the critical damping. This is the nominal value of damping for many actual structures. The magnification factor for acoustic modes Q_{ac} is chosen as 25, which corresponds to 2 percent of the critical damping. Reference 14 suggests this value of the magnification factor for acoustically treated enclosed spaces in the low-frequency range.

In order to provide a partial check of the structural part of the present analysis, natural frequencies of a simply supported, externally stiffened shell were calculated and compared with experimental results from reference 15. The experimental model had longitudinal stiffeners integrally built into the shell. As shown in figure 4, the agreement between analytical and experimental frequencies for this check case is good.

10

Natural Frequencies of Structure and Acoustic Field

Analytical natural frequencies of both fuselages are shown in figure 5. In calculating the results, all the modes in the frequency range studied are included (0 to 500 Hz); however, to simplify figure 5, not all of the modal frequencies are included. Figure 5 shows that the structural modal spectrum is significantly different for the two aircraft. For example, the lowest natural frequency is about 28 Hz for fuselage 1 and about 108 Hz for fuselage 2, and fuselage 1 has more modes (approximately 250) than does fuselage 2 (13) in the frequency range.

The acoustic mode frequencies of the fuselage interior space are shown in figure 6. As in the case of structural modes, all the acoustic modes in the frequency range studied were included in the calculations (0 to 500 Hz); however, not all modes are shown in figure 6. Fuselage 1 had more acoustic modes in the frequency range studied (1200) than fuselage 2 (47). The fuselage interior space receives acoustic energy in its acoustic modes, which are excited by the fuselage structural modes. For the particular end conditions assumed, the mnth acoustic mode will respond only to a structural mode having the same m and n numbers. (For other end conditions, the coupling between structural and acoustic modes is more complicated, as discussed in ref. 10.) In addition, when the natural frequencies of such mode pairs are close together, noise transmission into the fuselage interior takes place very efficiently. From the complicated nature of the modal frequency curves shown in figures 5 and 6, it can be seen that many such frequency matchings may occur. A search of the tabulated values of the modal frequencies revealed that approximate frequency matchings occurred for fuselage 1 at the following values:

m	n	s	ω_{mn}	ω_{mns}
1	1	0	46.3	51.3
1	6	0	218.7	204.1
2	6	0	218.0	205.0
2	8	1	388.6	384.0
3	2	0	88.0	89.7
3	8	1	388.0	385.0
4	8	1	387.5	386.2
5	8	1	387.5	387.7

For fuselage 2, such frequency matchings occurred only at

m	n	s	ω_{mn}	ω_{mns}
2	2	0	269.7	270.2

The relation of these frequency matchings to the noise reduction will be discussed later.

Noise Reduction

Numerical results for the interior noise are calculated from equations (15) and (16) and are presented in the form of noise reduction, which is defined as

$$\text{Noise reduction} = 10 \log_{10}\left(\overline{p_e^2}\Big/\overline{p^2}\right) \tag{17}$$

where $\overline{p_e^2}$ is the mean-square excitation pressure and $\overline{p^2}$ is the space-averaged mean-square interior noise pressure. The frequency range considered in the present study is from 0 to 500 Hz, since this range covers the blade passage frequency and the first few harmonics which are the predominant frequencies exciting the structure. In the results shown in figures 7 to 12, noise reduction is studied as a continuous function of excitation frequency, for a number of sweep velocities. It is noted that an interior noise spectrum actually consists of tones at the blade passage frequency and its harmonics. The noise reduction at those corresponding frequencies can be obtained from the continuous noise reduction plot. Sweep velocity is a function of the propeller rotational speed and the distance from the propeller center to the fuselage sidewall. Hence, when the propeller rotation or the propeller center relative to the fuselage sidewalls are altered, the sweep velocity is affected and a different noise reduction plot must be computed.

To illustrate the effect of blade passage frequency on noise reduction, a plot of noise reduction against frequency is shown in figure 7. The blade passage frequency is denoted as f_1 Hz. The noise reductions at f_1 and its higher harmonics are marked with circular symbols. If the blade passage frequency is changed to f_1^* (either by changing the number of blades in the propeller or the speed of rotation of the propeller) but the sweep velocity V is kept constant, the resulting discrete frequency spectrum of noise reduction associated with f_1^* and its harmonics changes as indicated by the square symbols in figure 7. Sweep velocity can be held constant by adjusting the distance between the propeller center and the fuselage sidewalls. It is seen from figure 7 that, by changing the blade passage frequency, the noise reduction changes significantly, depending on whether it and its harmonics lie near resonances or away from resonances. Hence, noise reduction is very sensitive to blade passage frequency and structural and acoustic resonances.

The effect of sweep velocity on the noise reduction is shown in figures 8(a) and 8(b) for fuselage 1 and fuselage 2, respectively. The entire surface area of the fuselages is exposed to noise excitation as shown in figure 8. Noise reduction is plotted against nondimensional frequency, with the reference frequency f_r as the nondimensionalizing frequency. The reference frequency is the frequency of $m = 1$, $n = 0$, shell mode obtained as described in appendix A. This reference frequency is approximately equal to the ring frequency discussed in reference 14. It is seen from figure 8(a) that, when the excitation is uniform (sweep velocity $V = \infty$ in eqs. (9)), noise reduction is a minimum at the reference frequency, whereas when the exciting pressures are sweeping around the fuselage sidewalls the noise reduction at this frequency is considerably higher. At frequencies below $f/f_r = 0.5$, however, noise

reduction is higher for uniform excitation than for the case of excitation with sweep velocity. For the case of uniform excitation, covering the full circumference of the fuselage (that is, $b_2 = \Pi R$ and $b_1 = 0$), the integrals I_{mni} are zero except when $n = 0$, and hence, for uniform excitation, only $n = 0$ structural modes are excited and transmit noise to the fuselage interior. The dip in the noise-reduction curve at the reference frequency for the case of uniform excitation in figure 8(a) may be explained by the large number of structural modes near this frequency as compared to other frequencies, as shown in figure 5. The dips in this curve below the reference frequency are due to the presence of acoustic modes only. In figure 8(b), for the frequency range shown, the noise reduction for uniform excitation is always higher than it is when sweep velocity is present. A comparison with figure 8(a) shows that this behavior is similar to that of fuselage 1 in the frequency range where $(f/f_r) < 0.5$. From figures 8(a) and 8(b), it is seen that the effect of sweep velocity on noise reduction is quite significant, often making a difference of 25 dB in comparison with uniform excitation.

The variation of noise reduction with sweep velocity is shown in figures 9(a) and 9(b) for fuselage 1 and fuselage 2, respectively. Only a portion of the fuselage surface area is exposed to excitation, in the vicinity of the propeller plane, as shown in figures 9(a) and 9(b). It is seen from these figures that, when the sweep velocity is reduced from 341.4 m/sec to 136.6 m/sec, the noise reduction increases by about 10 dB. These velocities are chosen due to the fact that many propellers have tip speeds in this range. The same trend of noise reduction, decreasing with increasing sweep velocities, has been observed to be generally maintained over a broad range of sweep velocities. This trend is shown in figures 10(a) and 10(b), for fuselage 1 and fuselage 2, respectively, where the noise reduction is plotted against sweep velocity at a few representative resonance frequencies.

The effect of changing the axial length exposed to noise excitation on noise reduction is shown in figures 11(a) and 11(b) for fuselage 1 and fuselage 2, respectively. It is seen from both the figures that at most frequencies the noise reduction is greater by as much as 10 dB when a smaller portion of fuselage length is subjected to excitation. An exception is shown in figure 11(b) at about 270 Hz where the noise reduction is substantially less when a smaller length of fuselage is excited. As indicated previously, the structural and acoustic modes with $m = 2$ and $n = 2$ have nearly the same frequencies, resulting in a matching of their resonances and consequently a low noise reduction. This low noise reduction does not occur when the whole fuselage is excited because the $m = 2$ axial modes are orthogonal to the uniform excitation distribution. It is also interesting to note that the dips in the noise-reduction curve in figure 11(a) correspond with the modal frequencies discussed earlier where structural and acoustic modal frequencies match.

The effect of circumferential pressure distribution on noise reduction is shown in figures 12(a) and 12(b) for fuselage 1 and fuselage 2, respectively. In these figures noise reductions are plotted for two different circumferential areas exposed to noise excitation, keeping the axial portion exposed to noise and the sweep velocity constant. A comparison of the two curves in figure 12(a) shows that the noise reduction does not vary substantially with circumferential

13

area for most frequencies. In figure 12(b) noise reduction is higher by as much as 20 dB when the circumferential area exposed to noise is reduced. These results indicate that, in general, it is important to have a knowledge of the distribution of noise in order to determine properly the noise reduction in a fuselage.

CONCLUDING REMARKS

The effect on noise reduction of propeller noise characteristics has been studied for a twin-engine, propeller-driven aircraft with two propellers rotating in opposite directions. The fuselage is modeled as a cylindrical shell with stringers and ring frames, whose effects are averaged over the fuselage surface. The mathematical model of the propeller noise excitation used in this study includes some of the propeller noise characteristics such as pressure waves sweeping around the fuselage sidewalls due to propeller rotation and the localized nature of excitation with the highest levels near the propeller plane. The influence of the propeller noise characteristics on the noise reduction is studied.

The results of this investigation show that substantial changes in noise reduction occurred when sweep velocity and area of fuselage subjected to noise excitation were changed. Noise reduction generally decreased as the sweep velocity increased. Reducing the area exposed to excitation generally increased noise reduction. For the range of variables studied, differences in noise reduction of the order of 10 to 20 dB were observed.

Langley Research Center
National Aeronautics and Space Administration
Hampton, VA 23665
October 13, 1978

APPENDIX A

EQUATION OF MOTION OF THE FUSELAGE STRUCTURE

In the differential equation of dynamic equilibrium for the fuselage structure, Donnell-type strain displacement relations for the cylinder (ref. 13) and beam-type strain displacement relations for the stiffeners are considered. Inplane inertias are neglected since they do not significantly influence the radial modes of the shell, which are of interest in this investigation. The equations of motion for an element of the smeared shell can be written as

$$L_{11}u + L_{12}v + L_{13}w = 0 \tag{A1a}$$

$$L_{21}u + L_{22}v + L_{23}w = 0 \tag{A1b}$$

$$L_{31}u + L_{32}v + L_{33}w = \left[-\frac{\rho_a(1 - \mu^2)}{E} \right]\left(\frac{\partial^2 w}{\partial t^2}\right) + \frac{p_e(x,y,t)}{Eh}(1 - \mu^2) \tag{A1c}$$

where u, v, and w are shell displacements in the x-, y-, and z-directions, respectively, h is the shell thickness, E is the modulus of elasticity of the shell material, μ is Poisson's ratio, t is the time, and $p_e(x,y,t)$ is the excitation pressure on the fuselage surface. The term ρ_a is the average density of the fuselage material given by

$$\rho_a = \rho + \frac{\rho_s A_s}{h \ell_s} + \frac{\rho_r A_r}{h \ell_r} \tag{A2}$$

The differential operators L_{rs} in equations (A1) are as follows (see ref. 13):

$$L_{11} = \left[1 + \frac{E_s A_s (1 - \mu^2)}{Eh \ell_s} \right]\frac{\partial^2}{\partial x^2} + \left(\frac{1 - \mu}{2}\right)\frac{\partial^2}{\partial y^2} \tag{A3a}$$

$$L_{12} = L_{21} = \left(\frac{1 + \mu}{2}\right)\frac{\partial^2}{\partial x\ \partial y} \tag{A3b}$$

$$L_{13} = L_{31} = \frac{\mu}{R}\frac{\partial}{\partial x} - \frac{z_s E_s A_s (1 - \mu^2)}{Eh \ell_s}\frac{\partial^3}{\partial x^3} \tag{A3c}$$

15

$$L_{22} = \left(\frac{1 - \mu}{2}\right)\frac{\partial^2}{\partial x^2} + \left[1 + \frac{E_r A_r (1 - \mu^2)}{Eh l_r}\right]\frac{\partial^2}{\partial y^2} \tag{A3d}$$

$$L_{23} = L_{32} = \left[1 + \frac{E_r A_r (1 - \mu^2)}{Eh l_r}\right]\frac{1}{R}\frac{\partial}{\partial y} - \frac{z_r E_r A_r (1 - \mu^2)}{Eh l_r}\frac{\partial^3}{\partial y^3} \tag{A3e}$$

$$L_{33} = \frac{h^2}{12}\nabla^4 + \frac{1}{R^2}\left[1 + \frac{E_r A_r (1 - \mu^2)}{Eh l_r}\right]$$

$$+ \frac{E_s(1 - \mu^2)\left(I_s + z_s^2 A_s\right)}{Eh l_s}\frac{\partial^4}{\partial x^4} + \frac{E_r(1 - \mu^2)\left(I_r + z_r^2 A_r\right)}{Eh l_r}\frac{\partial^4}{\partial y^4}$$

$$- \frac{2z_r E_r A_r (1 - \mu^2)}{REh l_r}\frac{\partial^2}{\partial y^2} + \frac{(1 - \mu^2)}{Eh}\left(\frac{G_s J_s}{l_s} + \frac{G_r J_r}{l_r}\right)\frac{\partial^4}{\partial x^2 \partial y^2} \tag{A3f}$$

With simple supports at each end of the shell, the boundary conditions to be satisfied at $x = 0$ and L are

$$w = M_x = v = N_x = 0 \tag{A4}$$

where M_x is the moment resultant and N_x is the stress resultant in the x-direction. The boundary conditions in equation (A4) are satisfied by

$$u(x,y,t) = \bar{u}_1(t) \cos (m\pi x/L) \sin (ny/R) \tag{A5a}$$

$$v(x,y,t) = \bar{v}_1(t) \sin (m\pi x/L) \cos (ny/R) \tag{A5b}$$

$$w(x,y,t) = \bar{w}_1(t) \sin (m\pi x/L) \sin (ny/R) \tag{A5c}$$

and also by

$$u(x,y,t) = \bar{u}_2(t) \cos (m\pi x/L) \cos (ny/R) \tag{A6a}$$

$$v(x,y,t) = \bar{v}_2(t) \sin (m\pi x/L) \sin (ny/R) \tag{A6b}$$

$$w(x,y,t) = \bar{w}_2(t) \sin (m\pi x/L) \cos (ny/R) \tag{A6c}$$

where m is the number of longitudinal half waves, and n is the number of circumferential waves, as illustrated in figure 2.

The free-vibration problem is solved to obtain the natural frequencies ω_{mn} by putting $p_e(x,y,t)$ equal to zero in equation (A1c), combining equations (A1) and (A5), and solving the resulting simultaneous equations in $\bar{u}_1$, $\bar{v}_1$, and $\bar{w}_1$. The same frequency equation yielding the same set of natural frequencies ω_{mn} is also obtained by combining equations (A1) and (A6).

Since both equations (A5) and (A6) satisfy the equations of motion and boundary condition of the fuselage structure, a complete solution for the response of the shell will involve the summation of both sets of solutions. Accordingly, the solutions for u, v, and w are taken as

$$u(x,y,t) = \sum_{mni} U_{mni}(x,y) q_{mni}(t) \tag{A7a}$$

$$v(x,y,t) = \sum_{mni} V_{mni}(x,y) q_{mni}(t) \tag{A7b}$$

$$w(x,y,t) = \sum_{mni} W_{mni}(x,y) q_{mni}(t) \tag{A7c}$$

where $i = 1, 2$. In equations (A7), the subscript $i = 1$ corresponds to the set of solutions in equations (A5) and $i = 2$ corresponds to the set of solutions given in equations (A6) and

$$\left.\begin{aligned}
U_{mn1}(x,y) &= \cos (m\pi x/L) \sin (ny/R) \\
V_{mn1}(x,y) &= \sin (m\pi x/L) \cos (ny/R) \\
W_{mn1}(x,y) &= \sin (m\pi x/L) \sin (ny/R)
\end{aligned}\right\} \tag{A8}$$

$$\left.\begin{aligned}
U_{mn2}(x,y) &= \cos (m\pi x/L) \cos (ny/R) \\
V_{mn2}(x,y) &= \sin (m\pi x/L) \sin (ny/R) \\
W_{mn2}(x,y) &= \sin (m\pi x/L) \cos (ny/R)
\end{aligned}\right\} \tag{A9}$$

17

After combining equations (A7) and equations (A1), the first two equations (A1a) and (A1b) identically vanish, and equation (A1c), after simplifying and applying the orthogonal property of the normal modes, yields the equation of motion for the (mni) mode as

$$\ddot{q}_{mni}(t) + \omega_{mn}^2 q_{mni}(t) = \frac{F_{mni}(t)}{M_{mni}} \tag{A10}$$

since $i = 1$ and $i = 2$ yield the same natural frequencies ω_{mn}. The terms M_{mni} and F_{mni} are the generalized mass and force of the (mni) mode, respectively, given by

$$M_{mni} = \iint \rho_a h W_{mni}^2(x,y)\, dx\, dy \tag{A11}$$

and

$$F_{mni}(t) = \iint p_e(x,y,t) W_{mni}(x,y)\, dx\, dy \tag{A12}$$

The presence of light damping in the fuselage structure can be accounted for by adding a damping term in equation (A10) so that the equation of motion of the (mni) mode of the damped structure becomes

$$\ddot{q}_{mni}(t) + \frac{\omega_{mn}}{Q_{mni}} \dot{q}_{mni}(t) + \omega_{mn}^2 q_{mni}(t) = \frac{F_{mni}(t)}{M_{mni}} \tag{A13}$$

where Q_{mni} denotes the dynamic magnification factor at resonance for the (mni) mode. Equation (A13) is the same as equation (1) of the Analysis.

APPENDIX B

INTERIOR NOISE

The internal acoustic field is defined by the wave equation

$$\nabla^2 p = \frac{1}{c^2}\left(\frac{\partial^2 p}{\partial t^2}\right) \tag{B1}$$

and the boundary conditions. Assuming the process to be harmonic, the solution to the wave equation for acoustic pressure is

$$p(x,\phi,r,t) = \left[C_1 J_\eta(\alpha\hat{r}) + C_2 Y_\eta(\alpha\hat{r}) \right]$$

$$\times (\cos \eta\phi + C_3 \sin \eta\phi)(\sin \psi x + C_4 \cos \psi x)e^{i\omega t} \tag{B2}$$

where C_1, C_2, C_3, C_4 and ψ are constants of integration, J_η and Y_η are ηth order Bessel functions of the first and second kind, respectively, and

$$\left. \begin{array}{l} \alpha = kR\left[1 - (\psi/k)^2\right]^{1/2} \\[2mm] \hat{r} = (r/R) \\[2mm] k = (\omega/c) \end{array} \right\} \tag{B3}$$

and r, ϕ, and x denote the cylindrical coordinates along radial, circumferential, and axial directions, and c is the speed of sound in air.

For this problem open-end conditions are assumed for the fuselage, and hence the acoustic pressures are zero at $x = 0$ and $x = L$. Using these values in equation (B2)

$$\left. \begin{array}{l} C_4 = 0 \\[2mm] \psi = (\xi\pi/L) \end{array} \right\} \tag{B4}$$

For finite pressures at the center of the cylindrical section, C_2 must be zero. Hence, by summing up the contributions of all the modes, the interior pressure is obtained as

$$p(x,\phi,r,t) = \sum_{\xi\eta} C_1 J_\eta(\alpha\hat{r}) \left[\sin \frac{\xi\pi x}{L}(\cos \eta\phi + C_3 \sin \eta\phi)e^{i\omega t} \right] \qquad (B5)$$

where $\xi = 1, 2, \ldots, \infty$ and $\eta = 0, 1, 2, \ldots, \infty$. With the circumferential coordinate $\phi = (y/R)$ in equation (B5), the total pressure in the interior of the fuselage can be expressed as

$$p(x,y,r,t) = \sum_{\xi\eta j} C_{\xi\eta j} J_\eta(\alpha\hat{r}) \left[\phi_{\xi\eta j}(x,y) e^{i\omega t} \right] \qquad (B6)$$

where $j = 1, 2$ and

$$\left. \begin{array}{l} \phi_{\xi\eta 1}(x,y) = \sin (\xi\pi x/L) \sin (\eta y/R) \\[2em] \phi_{\xi\eta 2}(x,y) = \sin (\xi\pi x/L) \cos (\eta y/R) \end{array} \right\} \qquad (B7)$$

When the process is harmonic, the pressure p is related to the particle displacement in the radial direction w_a by the relation

$$w_a = \left(1/\rho_o\omega^2 \right)(\partial p/\partial r) \qquad (B8)$$

where ρ_o is the air density within the fuselage. This relation couples the structural and acoustic analyses. By equating the radial deflections of the shell and the particle displacement in the radial direction at $r = R$, it is possible to arrive at an expression for the interior noise pressure. Combining equation (B6) and equation (B8) the particle displacement in the radial direction at $r = R$ is

$$w_a(x,y,R,t) = \sum_{\xi\eta j} \frac{C_{\xi\eta j}\alpha}{\rho_o\omega^2 R} \left[J_\eta'(\alpha) \right] \left[\phi_{\xi\eta j}(x,y) e^{i\omega t} \right] \qquad (B9)$$

where $( )' = \frac{d}{dr}( )$. Equating $w_a(x,y,R,t)$ given in equation (B9) to $w(x,y,t)$ in equation (8), the values of the constants $C_{\xi\eta j}$ can be obtained by using the orthogonal property of the normal modes. It can be seen from equations (A7c), (A8), and (A9) and equations (B6) and (B7) that the space functions describing the shell radial deflections and the space functions describing the interior noise pressures at $r = R$ are similar, that is,

$$W_{mni}(x,y) = \phi_{mni}(x,y) \qquad (B10)$$

where $mni = \xi\eta j$. Using this result and the orthogonality property of the space functions, the modal constants C_{mni} are obtained as

$$C_{mni} = \frac{\rho_0 \omega^2 RP I_{mni} H(\omega/\omega_{mn}) e^{-\theta(\omega/\omega_{mn})}}{M_{mni} \omega_{mn}^2 \alpha J_n'(\alpha)} \tag{B11}$$

Substituting for C_{mni} from equation (B11) in equation (B6) the noise pressure in the fuselage interior is obtained as

$$p(x,y,r,t) = \rho_0 \omega^2 RP \sum_{mni} \left[\frac{H(\omega/\omega_{mn}) e^{-\theta(\omega/\omega_{mn})} I_{mni}}{M_{mni} \omega_{mn}^2 \alpha J_n'(\alpha)} \right] \left[J_n(\alpha\hat{r}) \right] \left[\phi_{mni}(x,y) e^{i\omega t} \right] \tag{B12}$$

In equation (B12) when $J_n'(\alpha) = 0$, the noise pressure goes to infinity. In an undamped acoustic field, subjected to finite excitations, pressure will go to infinity only at its natural frequencies. Hence, the roots of the equation

$$J_n'(\alpha) = 0 \tag{B13}$$

correspond to the natural frequencies of acoustic modes. If α_{ns} represents roots of equation (B13), then the natural frequencies of acoustic modes are obtained using equations (B3)

$$\omega_{mns} = \omega_m \left[1 + L^2 \left(\alpha_{ns}^2 / \pi^2 \right) m^2 R^2 \right]^{1/2} \tag{B14}$$

and

$$\omega_m = (m\pi c/L)$$

From equation (B12) the mean-square pressure is obtained as

$$\overline{p^2}(x,y,r,\omega) = \overline{P^2} \rho_0^2 R^2 \omega^4 \sum_{mni} \frac{\left| H(\omega/\omega_{mn}) \right|^2}{M_{mni}^2 \omega_{mn}^4} \left\{ \frac{J_n^2(\alpha\hat{r})}{\alpha^2 \left[J_n'(\alpha) \right]^2} \right\}$$

$$\times \left[\phi_{mni}^2(x,y) \left| I_{mni} \right|^2 \right] + \sum (\text{cross terms}) \tag{B15}$$

Space averaging the mean-square interior noise pressure, the cross terms in equation (B15) vanish due to the orthogonality of the modes, and hence the space-averaged mean-square pressure in the fuselage interior is obtained as

$$\overline{p^2}(\omega) = \overline{P^2}\rho_o^2 R^2 \omega^4 \sum_{mni} \frac{\left|H(\omega/\omega_{mn})\right|^2}{M_{mni}^2 \omega_{mn}^4} \left\{ \frac{\left|I_{mni}\right|^2 \gamma_{mni}}{\alpha^2 \left[J_n'(\alpha)\right]^2} \right\} \left[J_n^2(\alpha) - J_{n-1}(\alpha)J_{n+1}(\alpha)\right] \tag{B16}$$

for $\omega_m < \omega$ where

$$\gamma_{mni} = \frac{1}{2\pi RL} \iint \phi_{mni}^2(x,y)\, dx\, dy \tag{B17}$$

Since $\alpha = kR\left[1 - (\omega_m/\omega)\right]^{1/2}$, α becomes imaginary when $\omega_m > \omega$, in which case the equation (B16) becomes

$$\overline{p^2}(\omega) = \overline{P^2}\rho_o^2 R^2 \omega^4 \sum_{mni} \frac{\left|H(\omega/\omega_{mn})\right|^2 \left|I_{mni}\right|^2 \gamma_{mni}}{M_{mni}^2 \omega_{mn}^4 |\alpha|^2 \left[I_n'(|\alpha|)\right]^2} \left[I_n^2(|\alpha|) - I_{n-1}(|\alpha|)I_{n+1}(|\alpha|)\right] \tag{B18}$$

for $\omega_m > \omega$ where I_n represents modified Bessel functions of the first kind.

So far in the analysis, damping has not been considered for the acoustic modes, and hence the interior pressure will tend to infinity when $J_n'(\alpha) \to 0$. Damping in the acoustic modes is introduced as explained in reference 10. The term $J_n'(\alpha)$ is expanded in a series around those points where $J_n'(\alpha) = 0$; that is,

$$J_n'(\alpha) = J_n'(\alpha_{ns}) + (\alpha - \alpha_{ns})\left[J_n''(\alpha_{ns})\right] + \cdots \tag{B19}$$

Since $J_n'(\alpha_{ns}) = 0$, equation (B19) can be written as

$$J_n'(\alpha) \approx (\alpha - \alpha_{ns})J_n''(\alpha_{ns}) \tag{B20}$$

where the series in equation (B19) is truncated after the second term. For small values of $(\alpha - \alpha_{ns})$,

$$\alpha^2 - \alpha_{ns}^2 \approx 2\alpha_{ns}(\alpha - \alpha_{ns}) \tag{B21}$$

Substituting $\alpha^2 = \omega^2 \dfrac{R^2}{c^2}\left[1 - (\omega_m/\omega)^2\right]$ and $\alpha_{ns}^2 = \omega_{mns}^2 \dfrac{R^2}{c^2}\left[1 - (\omega_m/\omega_{mns})^2\right]$ in equation (B21) it is seen that

$$\alpha - \alpha_{ns} \approx \frac{k^2 R^2 \left[1 - (\omega_{mns}/\omega)^2\right]}{2\alpha_{ns}} \tag{B22}$$

Using the relationships in equations (B20) and (B22),

$$\frac{1}{\alpha^2 \left[J_n'(\alpha)\right]^2} \approx \frac{4}{k^4 R^4 \left[J_n''(\alpha_{ns})\right]^2 \left[1 - \left(\dfrac{\omega}{\omega_{mns}}\right)^2\right]} \tag{B23}$$

where $\alpha \to \alpha_{ns}$. Inserting the acoustic dynamic magnification factor Q_{ac} and allowing $\omega \to \omega_{mns}$, equation (B23) can be written as

$$\frac{1}{\alpha^2 \left[J_n'(\alpha)\right]^2} \approx \frac{4Q_{ac}^2}{k^4 R^4 \left[J_n''(\alpha_{ns})\right]^2} \tag{B24}$$

Substituting the value of $(1/\alpha^2)\left[J_n'(\alpha)\right]^2$ given in equation (B24) into equation (B16), the space-averaged mean-square interior noise pressure in the vicinity of acoustic resonances is obtained as

$$\overline{p^2}(\omega) = \overline{P^2}\rho_o^2 R^2 \omega^4 \sum_{mni} \frac{\left|H(\omega/\omega_{mn})\right|^2}{M_{mni}^2 \omega_{mni}^4} \frac{\left|I_{mni}\right|^2 \gamma_{mni}\left(4Q_{ac}^2\right)}{k^4 R^4 \left[J_n''(\alpha_{ns})\right]^2}\left[J_n^2(\alpha) - J_{n-1}(\alpha)J_{n+1}(\alpha)\right] \tag{B25}$$

for $\omega \to \omega_{mns}$.

23

REFERENCES

1. Hubbard, Harvey H.; and Regier, Arthur A.: Free-Space Oscillating Pressures Near the Tips of Rotating Propellers. NACA Rep. 996, 1950.

2. Deming, Arthur F.: Propeller Rotation Noise Due to Torque and Thrust. NACA TN 747, 1940.

3. Regier, Arthur A.; and Hubbard, Harvey H.: Status of Research on Propeller Noise and Its Reduction. J. Acoust. Soc. America, vol. 25, no. 3, May 1953, pp. 395-404.

4. Franken, Peter A.; Kerwin, Edward M., Jr.; and the Staff of Bolt Beranek and Newman, Inc.: Methods of Flight Vehicle Noise Prediction. WADC Tech. Rep. 58-343, ASTIA Doc. No. AD 205 776, U.S. Air Force, Nov. 1958.

5. Marte, Jack E.; and Kurtze, Donald W.: A Review of Aerodynamic Noise From Propellers, Rotors, and Lift Fans. Tech. Rep. No. 32-1462, Jet Propulsion Lab., California Inst. Technol., Jan. 1, 1970. (Available as NASA CR-107563.)

6. Ungar, Eric E.; Wilby, John F.; and Bliss, Donald B., et al.: A Review of Methods for Estimation of Aeroacoustic Loads on Flight Vehicle Surfaces. AFFDL-TR-76-91, U.S. Air Force, Feb. 1977. (Available from DDC as AD A042 783.)

7. Hanson, Donald B.: Near Field Noise of High Tip Speed Propellers in Forward Flight. AIAA Paper No. 76-565, July 1976.

8. Wilby, J. F.; and Scharton, T. D.: Acoustic Transmission Through a Fuselage Sidewall. NASA CR-132602, 1975.

9. Koval, L. R.: On Sound Transmission Into a Thin Cylindrical Shell Under "Flight Conditions." J. Sound & Vib., vol. 48, no. 2, Sept. 22, 1976, pp. 265-275.

10. Cockburn, J. A.; and Jolly, A. C.: Structural-Acoustic Response Noise Transmission Losses and Interior Noise Levels of an Aircraft Fuselage Excited by Random Pressure Fields. Tech. Rep. AFFDL-TR-68-2, U.S. Air Force, Aug. 1968.

11. Mixson, John S.; Barton, C. Kearney; and Vaicaitis, Rimas: Investigation of Interior Noise in a Twin-Engine Light Aircraft. J. Aircr., vol. 15, no. 6, Apr. 1978.

12. Vaicaitis, R.; and McDonald, W.: Noise Transmission Into a Light Aircraft. AIAA Paper 78-197, Jan. 1978.

13. Mikulas, Martin M., Jr.; and McElman, John A.: On Free Vibrations of
    Eccentrically Stiffened Cylindrical Shells and Flat Plates. NASA
    TN D-3010, 1965.

14. Beranek, Leo L., ed.: Noise and Vibration Control. McGraw-Hill Book Co.,
    Inc., c.1971.

15. Sewall, John L.; and Naumann, Eugene C.: An Experimental and Analytical
    Vibration Study of Thin Cylindrical Shells With and Without Longitudinal
    Stiffeners. NASA TN D-4705, 1968.

TABLE I.- STRUCTURAL DETAILS OF THE FUSELAGES
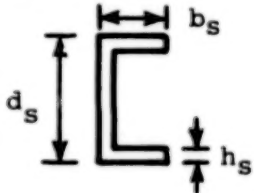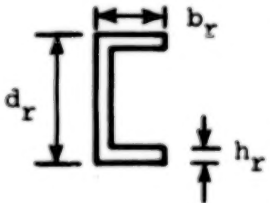
Dimension	Fuselage 1	Fuselage 2	Stiffener cross sections
Length, L, m	15.00	3.24	
Diameter, D, m	4.00	1.34	
Skin thickness, h, mm	1.00	.64	
Stringer thickness, h_s, mm	1.50	0.64	
Stringer depth, d_s, cm	4.00	1.91	
Stringer flange width, b_s, cm	2.00	1.42	
Stringer spacing, l_s, cm	18.00	7.62	
Frame thickness, h_r, mm	1.50	1.52	
Frame depth, d_r, cm	10.00	3.81	
Frame flange width, b_r, cm	4.00	1.91	
Frame spacing, l_r, cm	40.00	20.32	

TABLE II.- PROPERTIES OF MATERIALS

Modulus of elasticity of skin, stringer, and frame,
  E, E_r, E_s, Pa . . . . 0.71 × 10^{11}

Poisson's ratio, μ 0.33

Density of skin, stringer, and frame material,
  ρ, ρ_s, ρ_r, kg/m³ . . . . 0.27 × 10^4

Density of air, ρ_0, kg/m³ 1.25

Velocity of sound in air, c, m/sec 341.4

Magnification factor for structure, Q_{mni} 50

Magnification factor for air, Q_{ac} 25
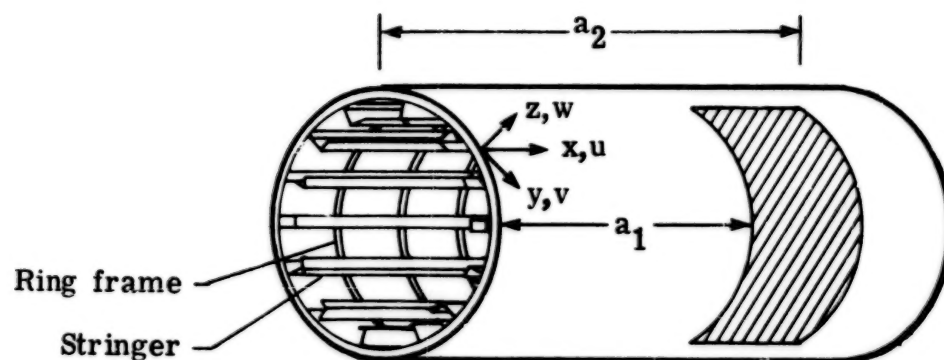
(a) Fuselage.
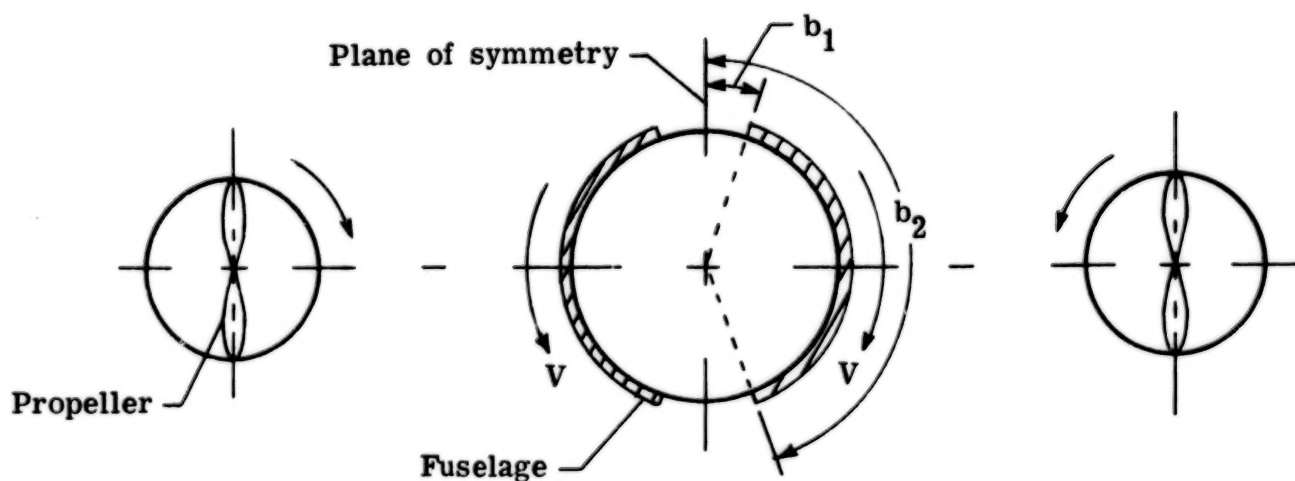
(b) Propeller noise distribution.

Figure 1.- Models showing fuselage and propeller noise distribution.
All dimensions are in meters.
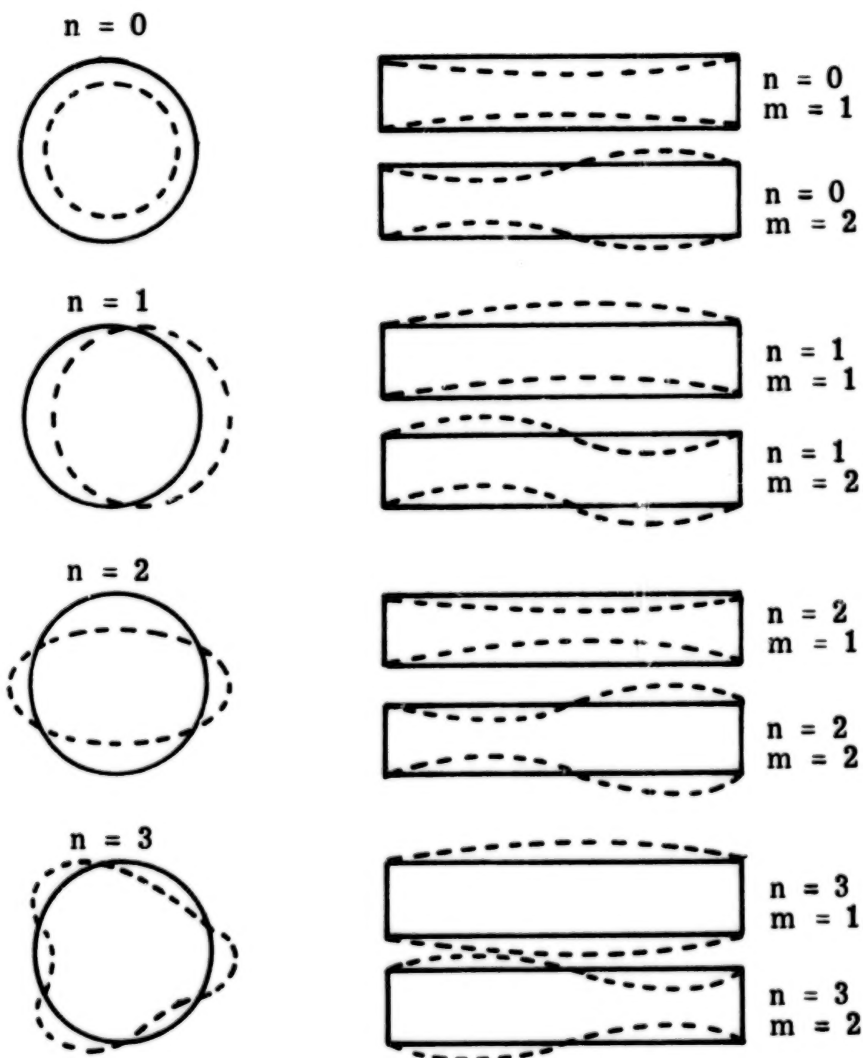
Figure 2.- Structural mode shapes of a cylindrical shell.
m indicates number of elastic half waves along cylinder
axis; n, number of elastic full waves around cylinder
circumference.
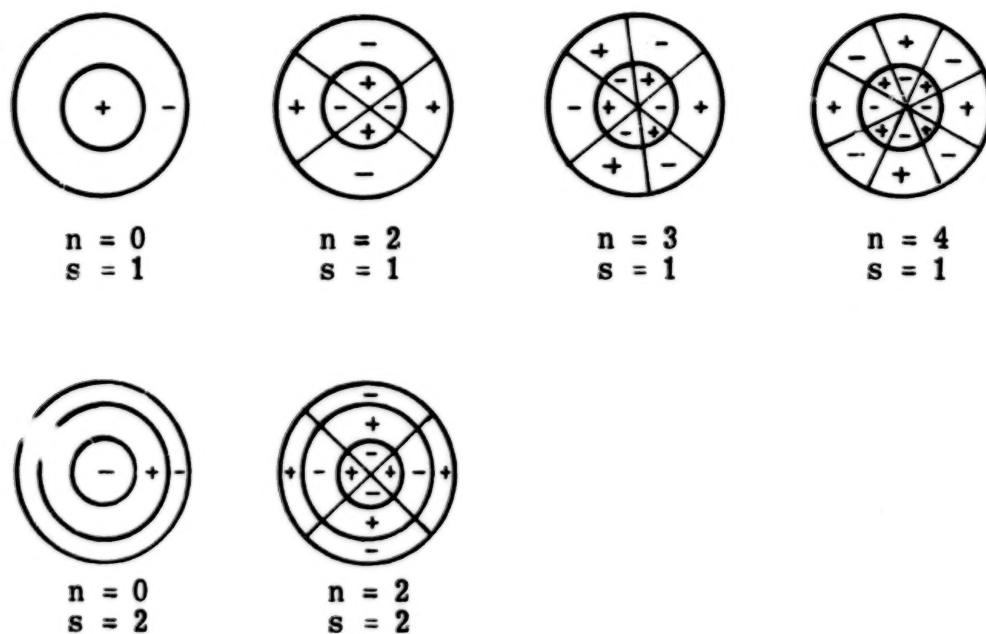
Figure 3.- Typical circumferential and radial acoustic node patterns. n indicates number of circumferential full waves; s, number of radial waves.
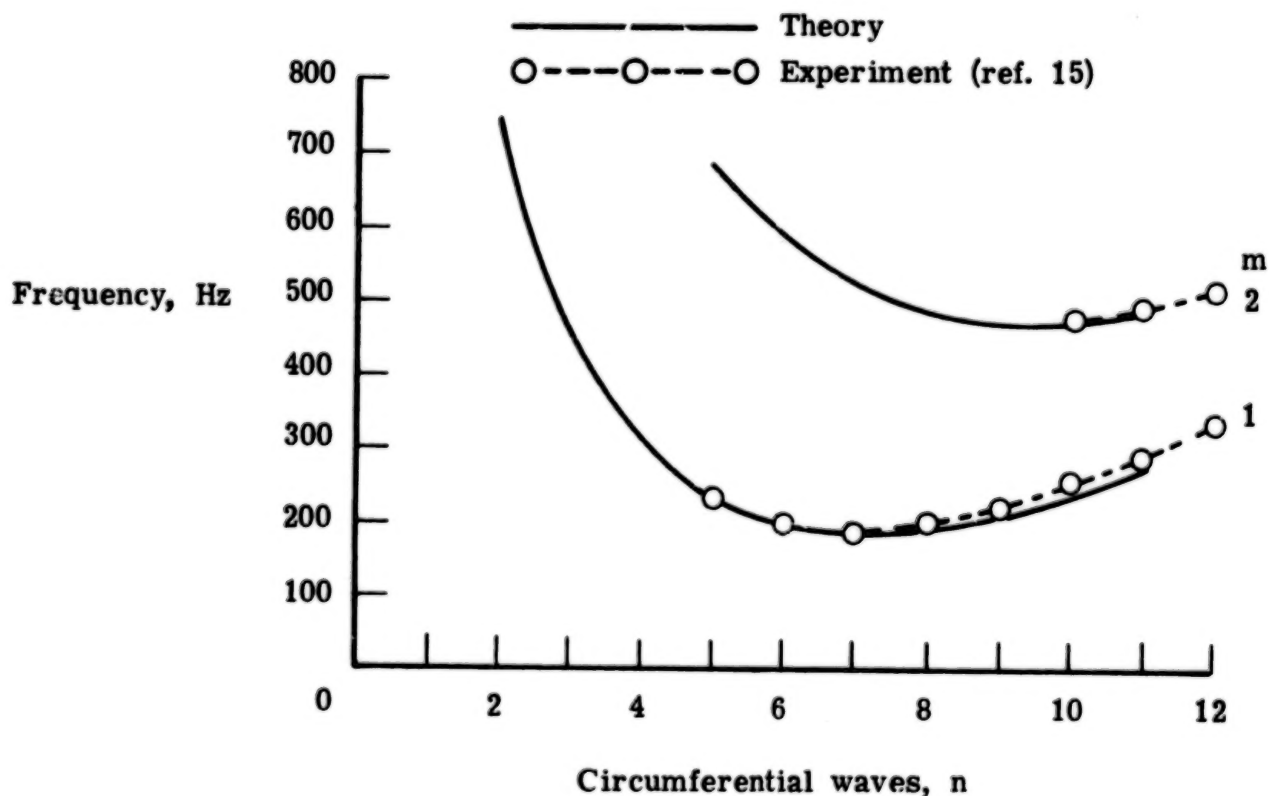
Figure 4.- Comparison of predicted and measured natural frequencies.
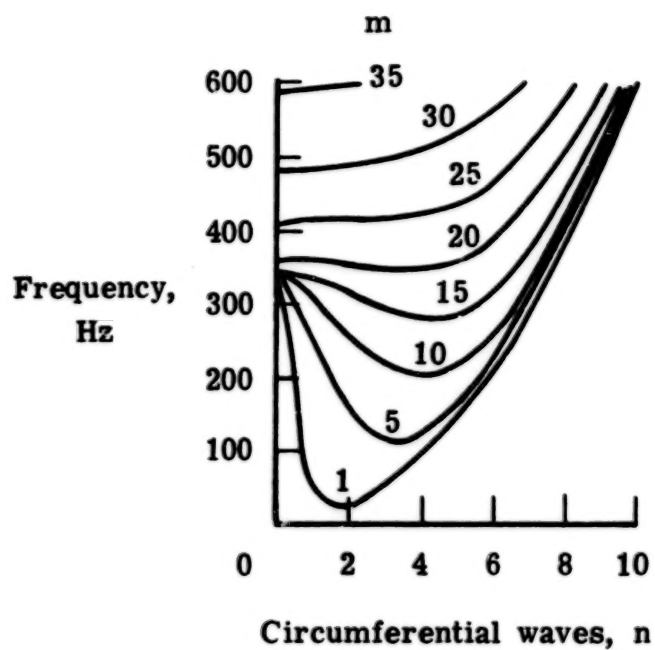
(a) Fuselage 1.
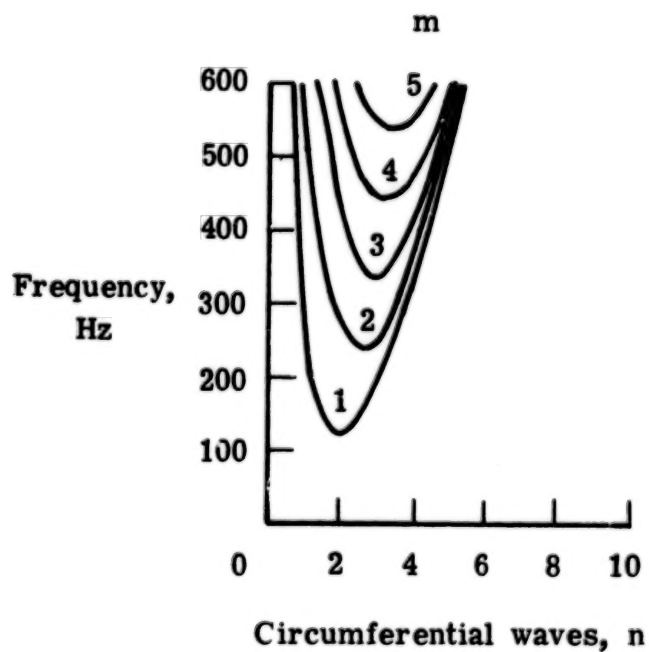
(b) Fuselage 2.

Figure 5.- Modal frequencies of fuselage structure.
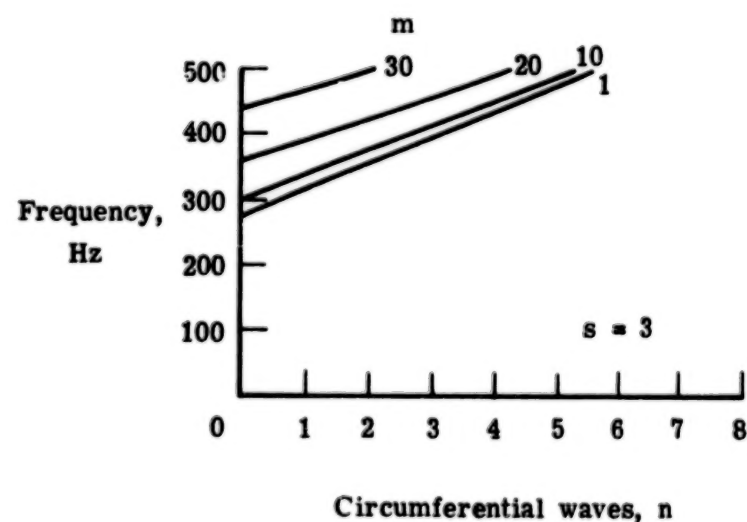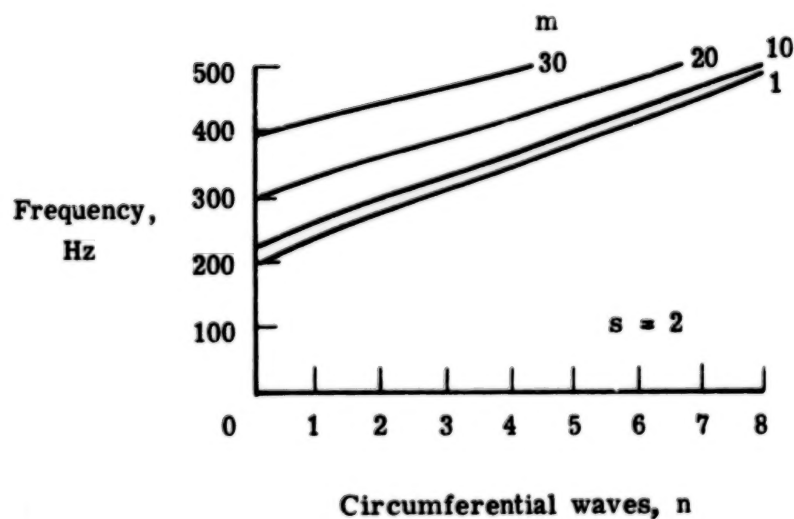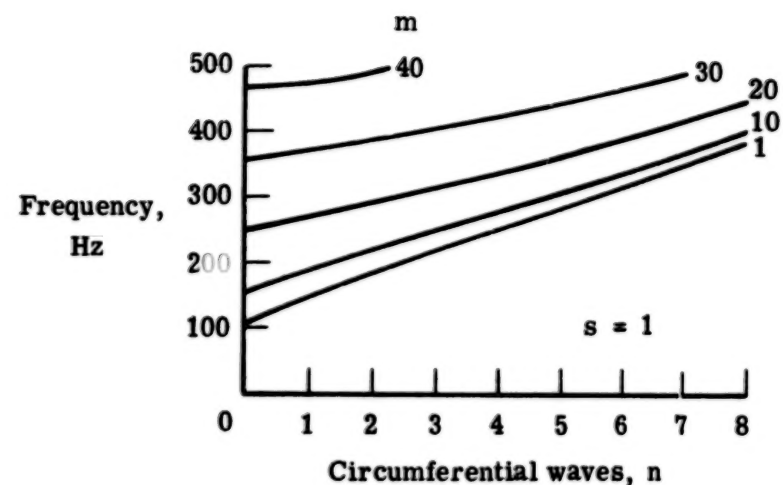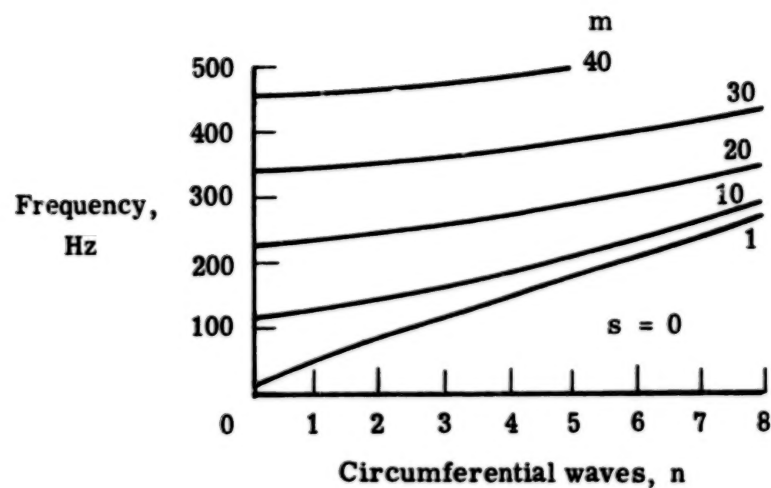
(a) Fuselage 1.

Figure 6.- Acoustic modal frequencies of fuselage interior space. m indicates number of longitudinal half waves; n, number of circumferential full waves; s, number of radial waves.
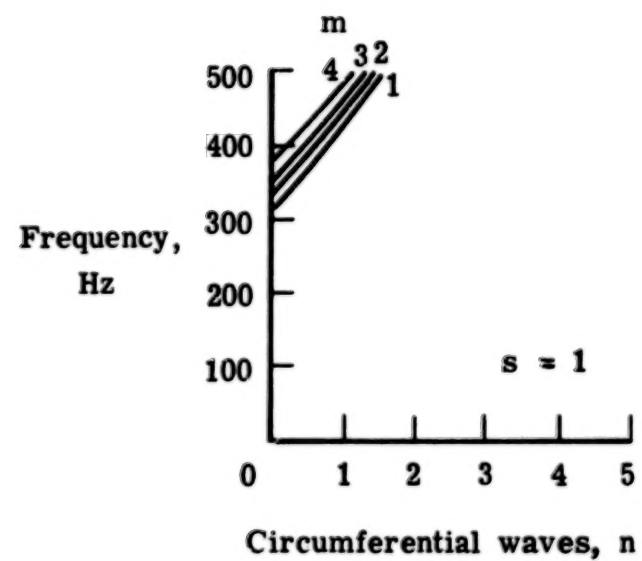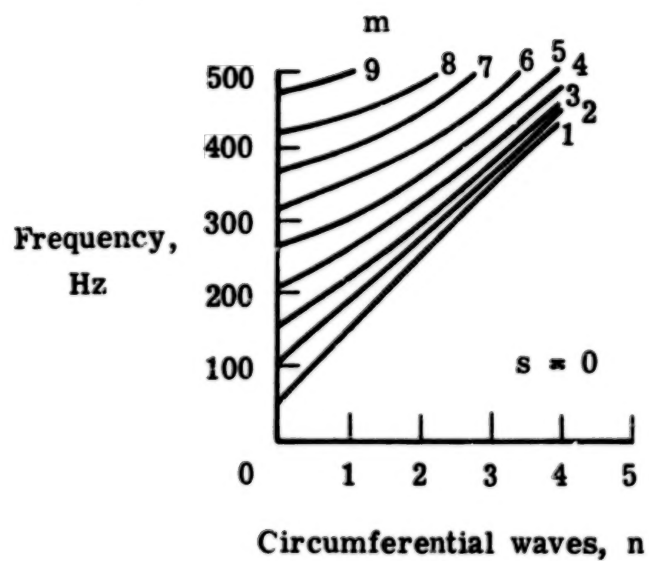
(b) Fuselage 2.

Figure 6.- Concluded.

33
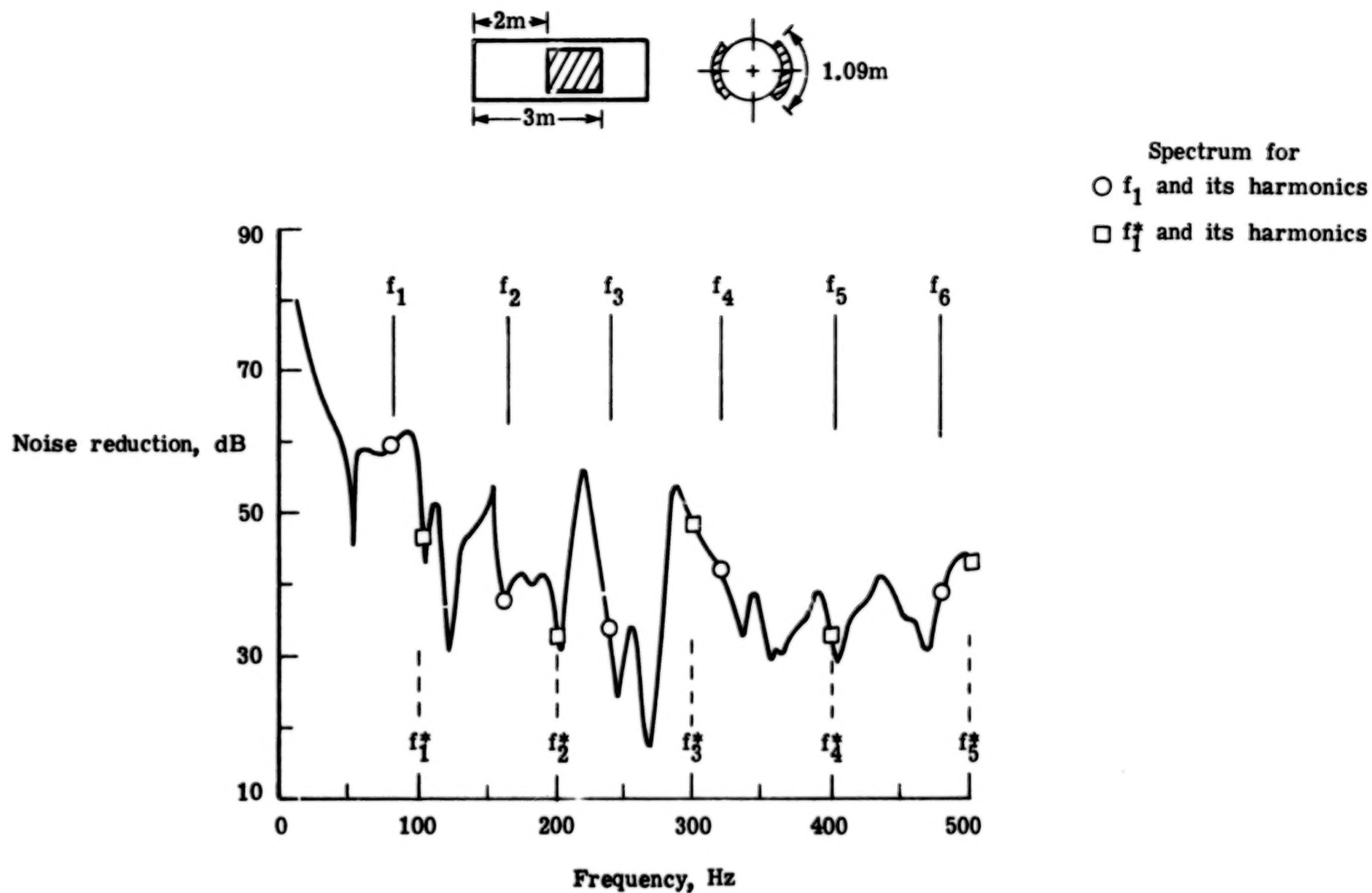
Figure 7.- Effect on noise reduction of changing blade passage frequency.
Fuselage 2; sweep velocity, $V = 68.4$ m/sec.

34
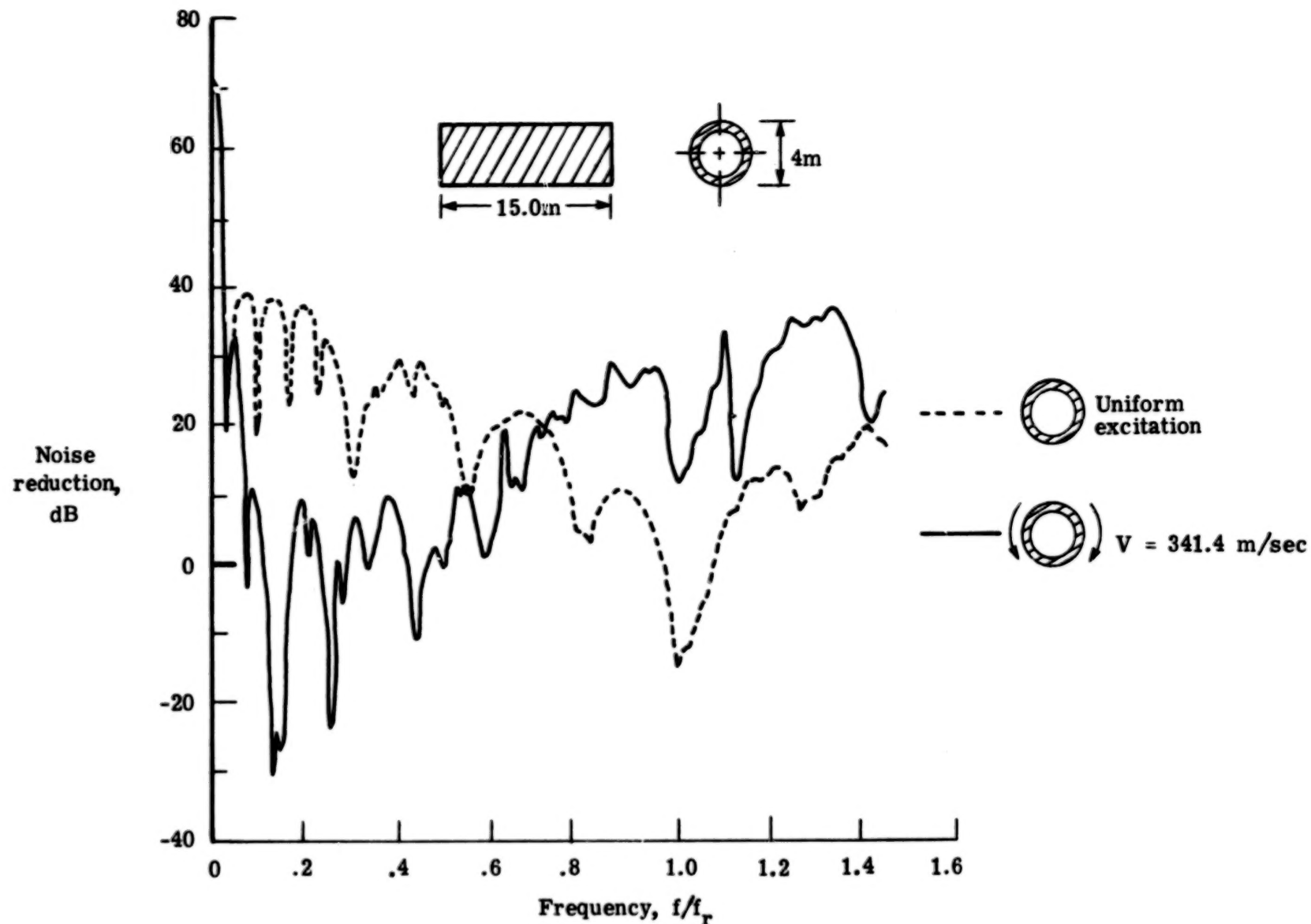
(a) Fuselage 1; exterior pressure distributed uniformly over
the whole fuselage; f_r = 347 Hz.

Figure 8.- Variation of noise reduction with excitation frequency with and
without sweep velocity.

35
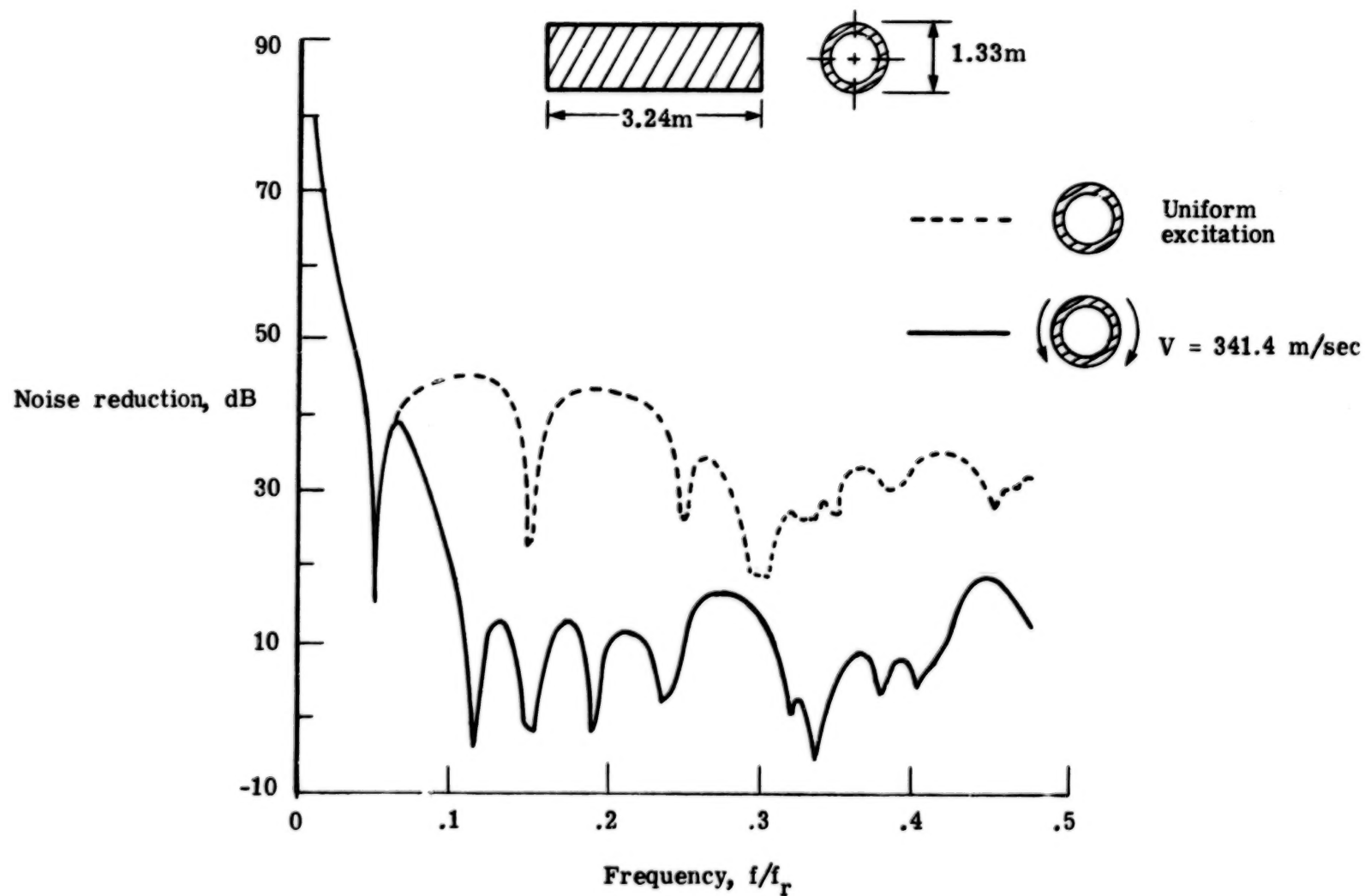
(b) Fuselage 2; exterior pressure distributed uniformly over the whole fuselage; f_r = 1056 Hz.

Figure 8.- Concluded.

36
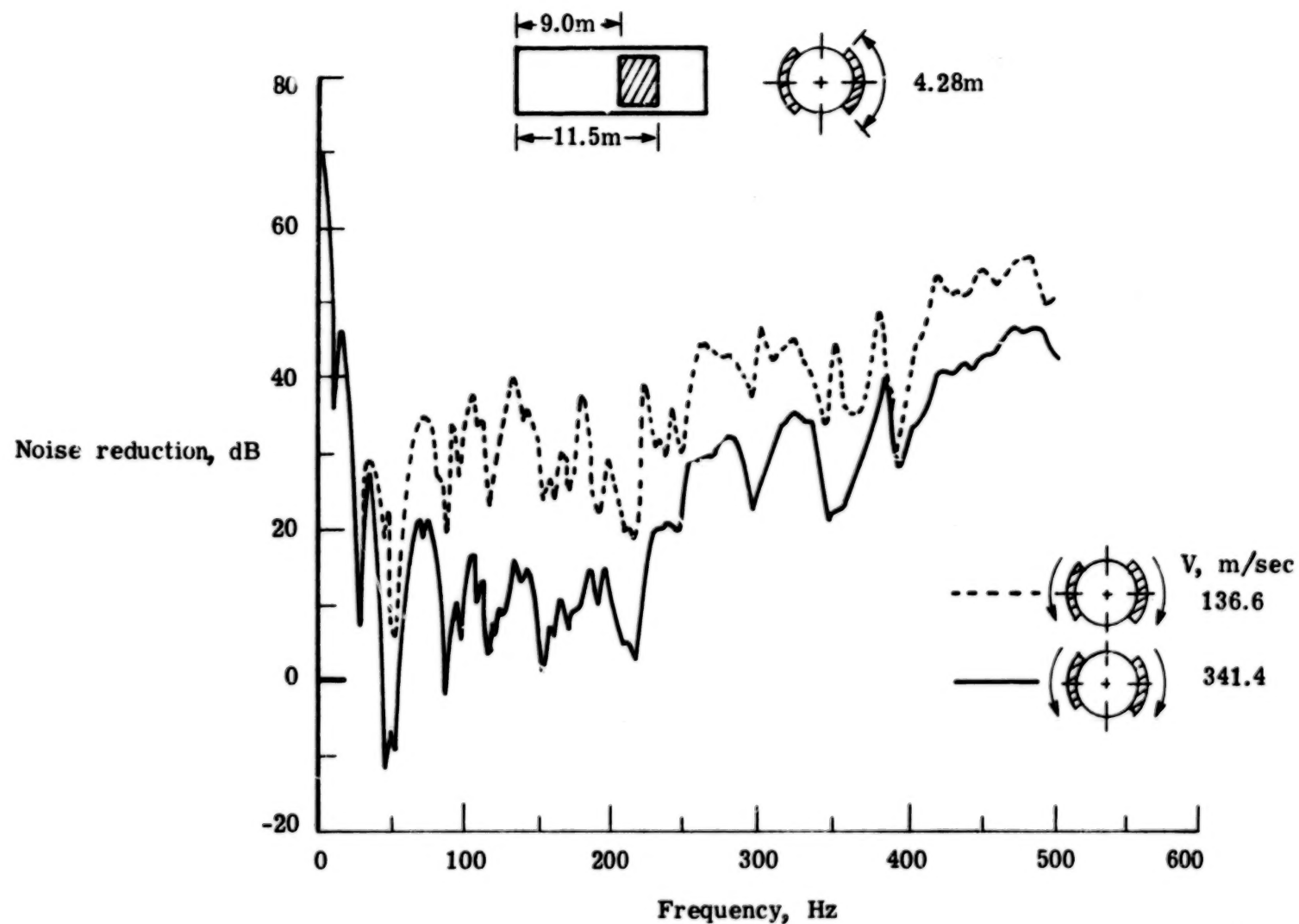
(a) Fuselage 1; exterior pressure on part of fuselage.

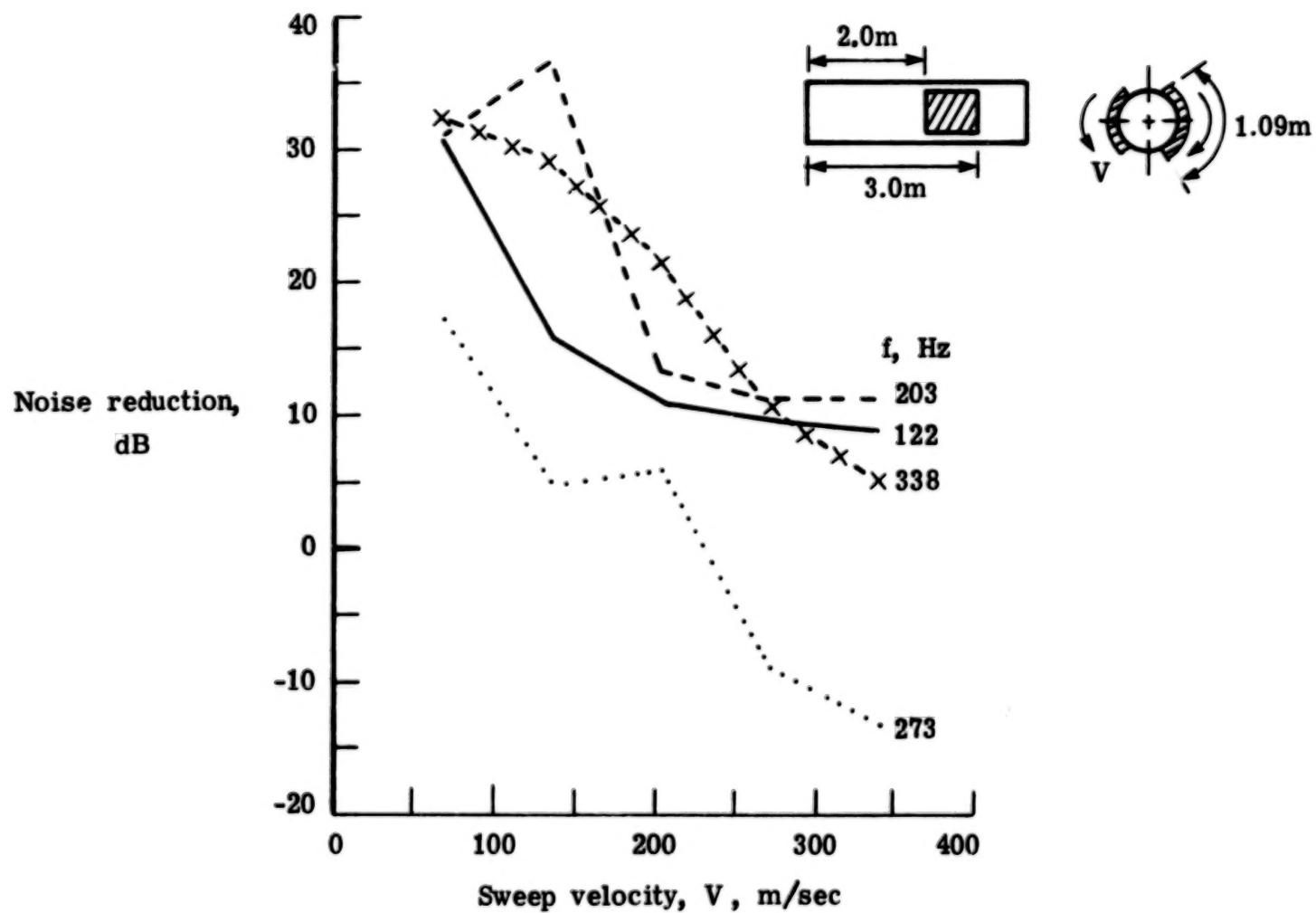Figure 9.- Variation of noise reduction with excitation frequency for two sweep velocities.

37
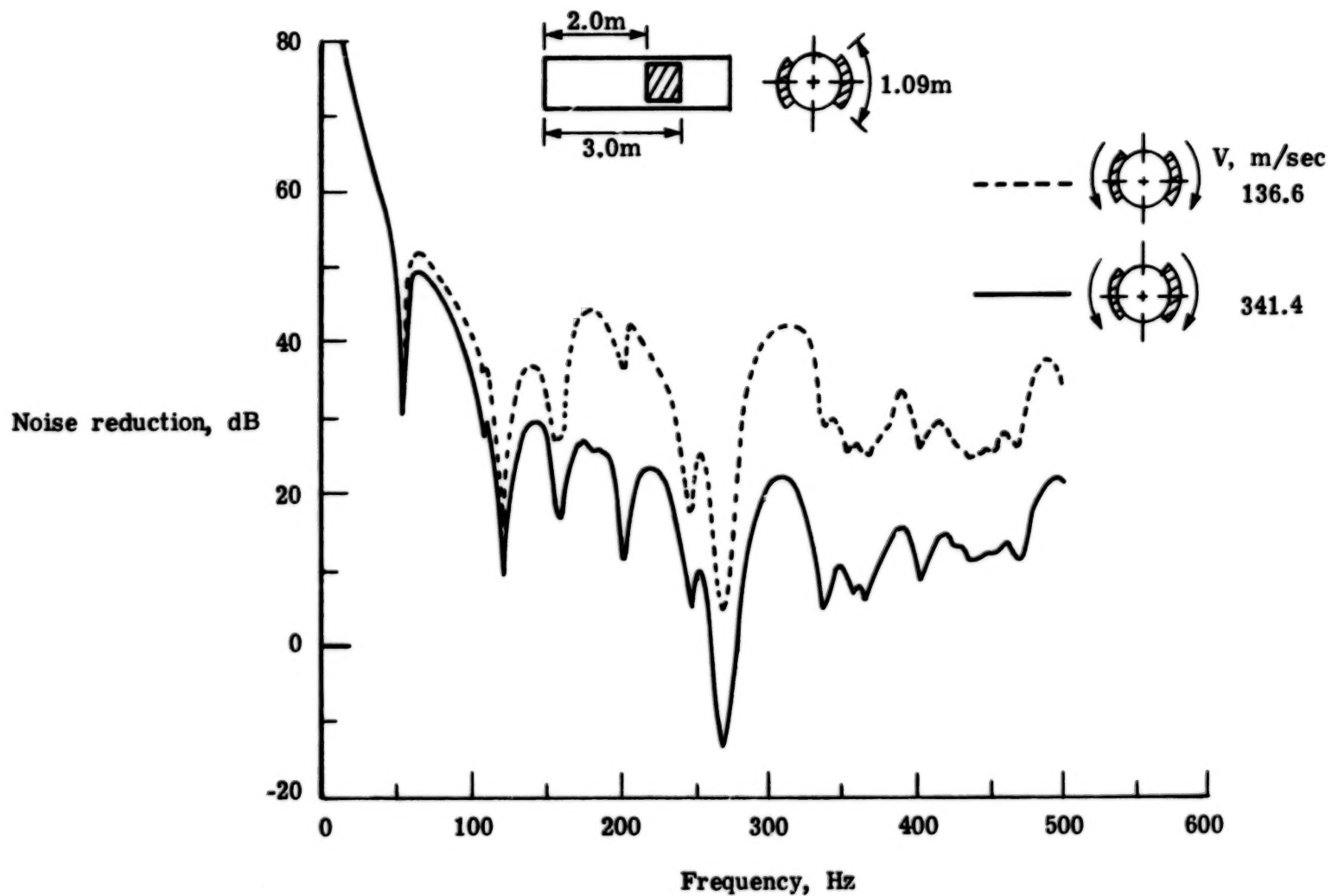
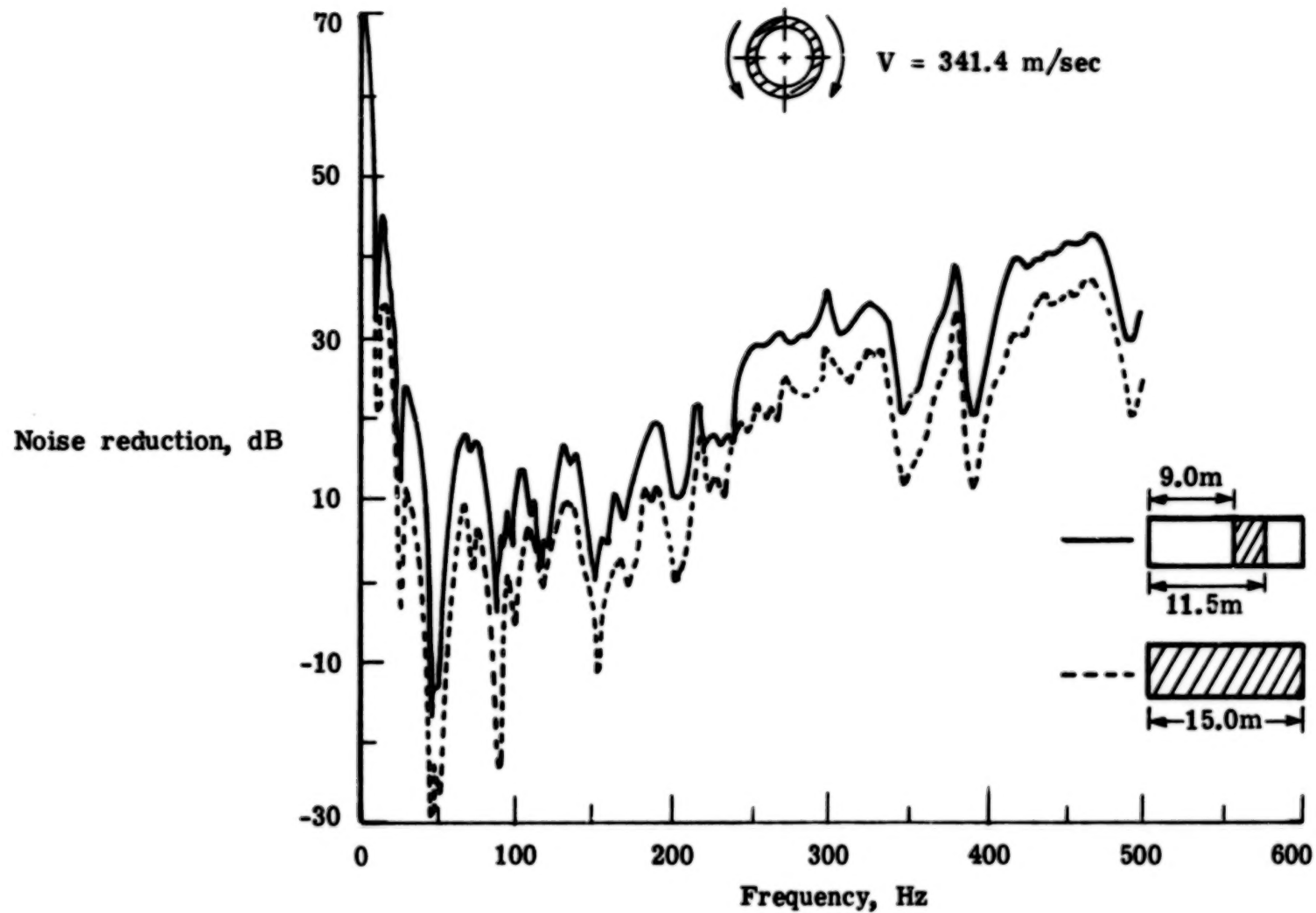(b) Fuselage 2; exterior pressure on part of fuselage.

Figure 9.- Concluded.
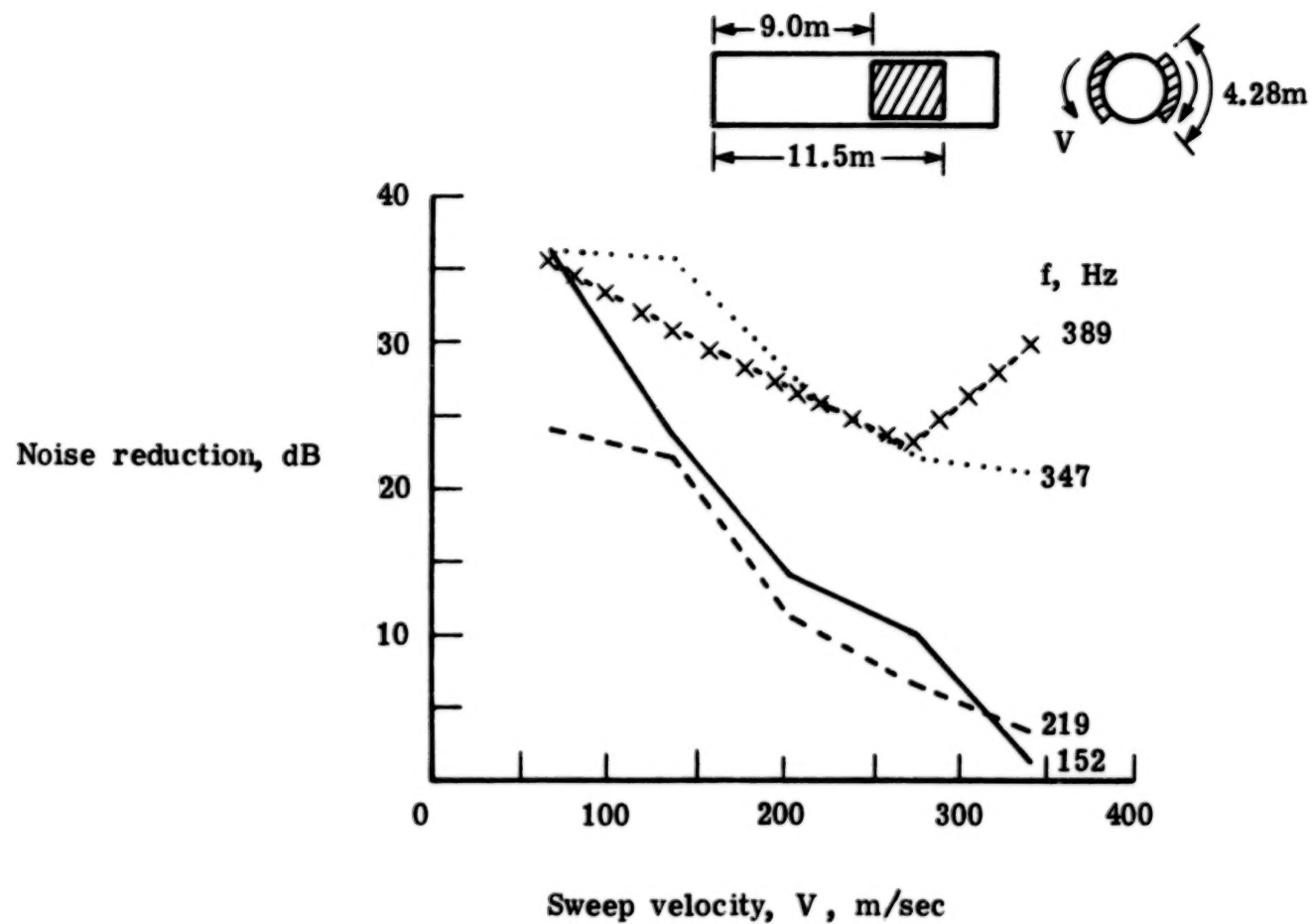
(a) Fuselage 1.

Figure 10.- Variation of noise reduction with sweep velocity
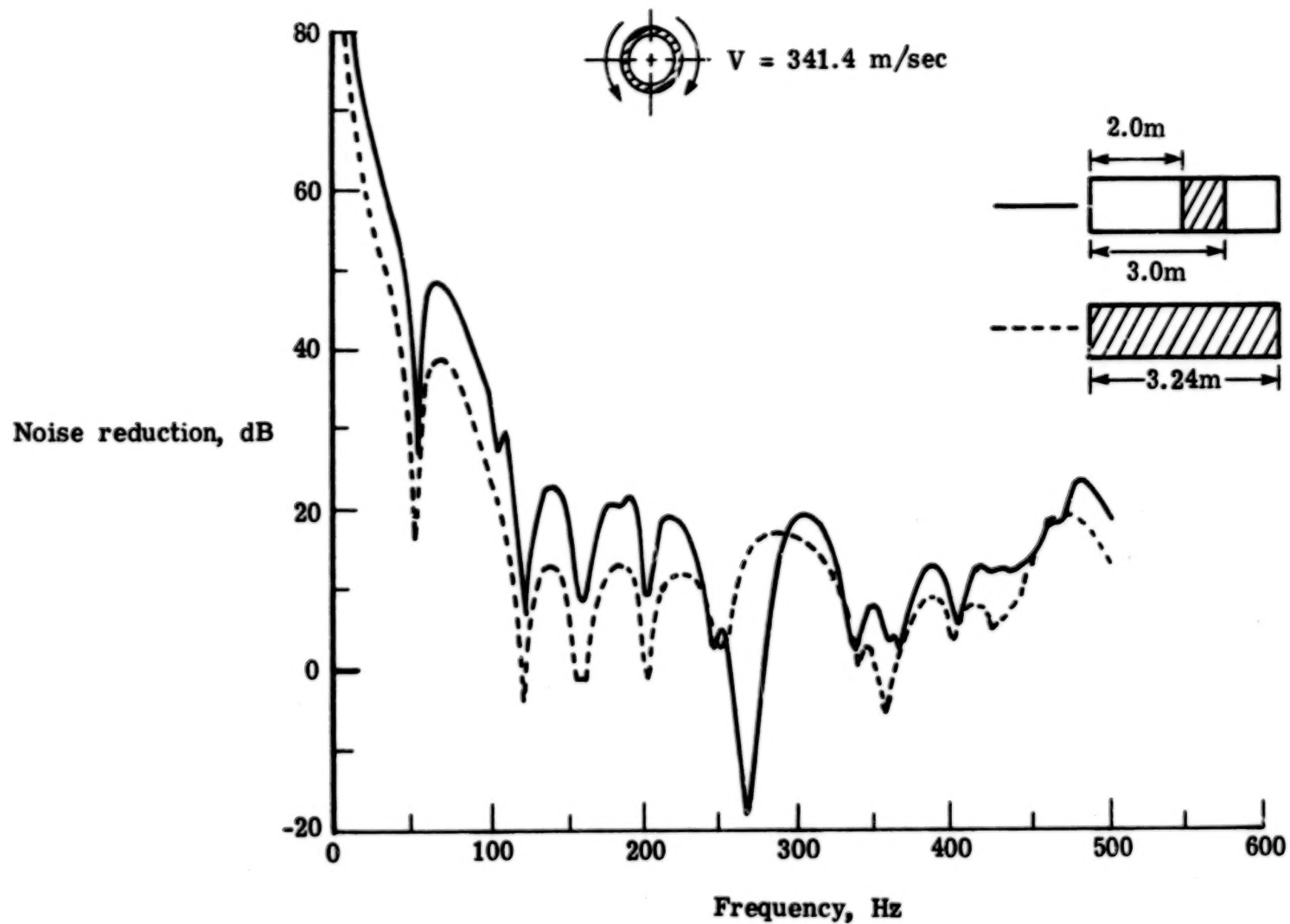at structural resonances.

39

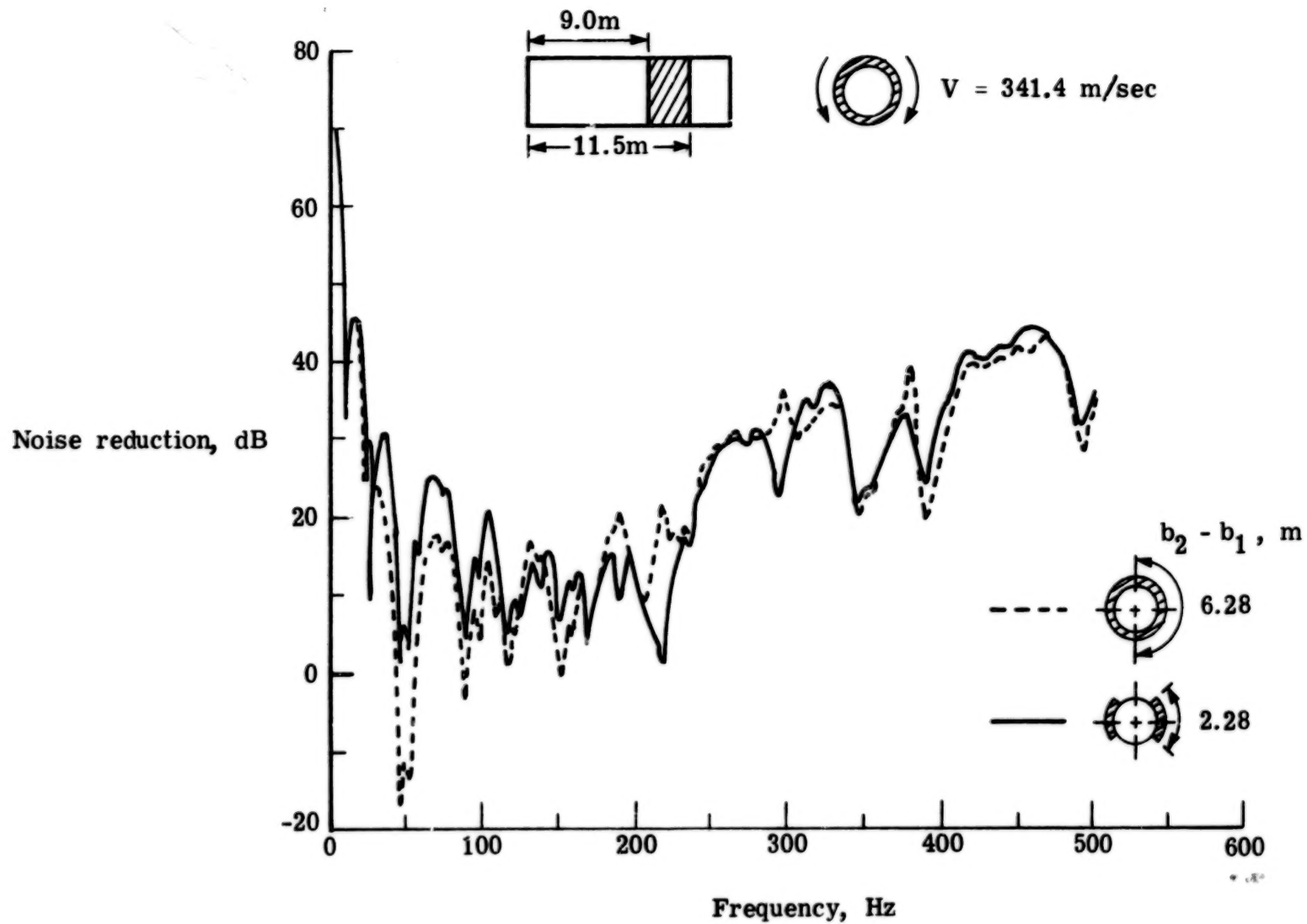(b) Fuselage 2.

Figure 10.- Concluded.

40

(a) Fuselage 1.

Figure 11.- Effect on noise reduction of reducing axial length
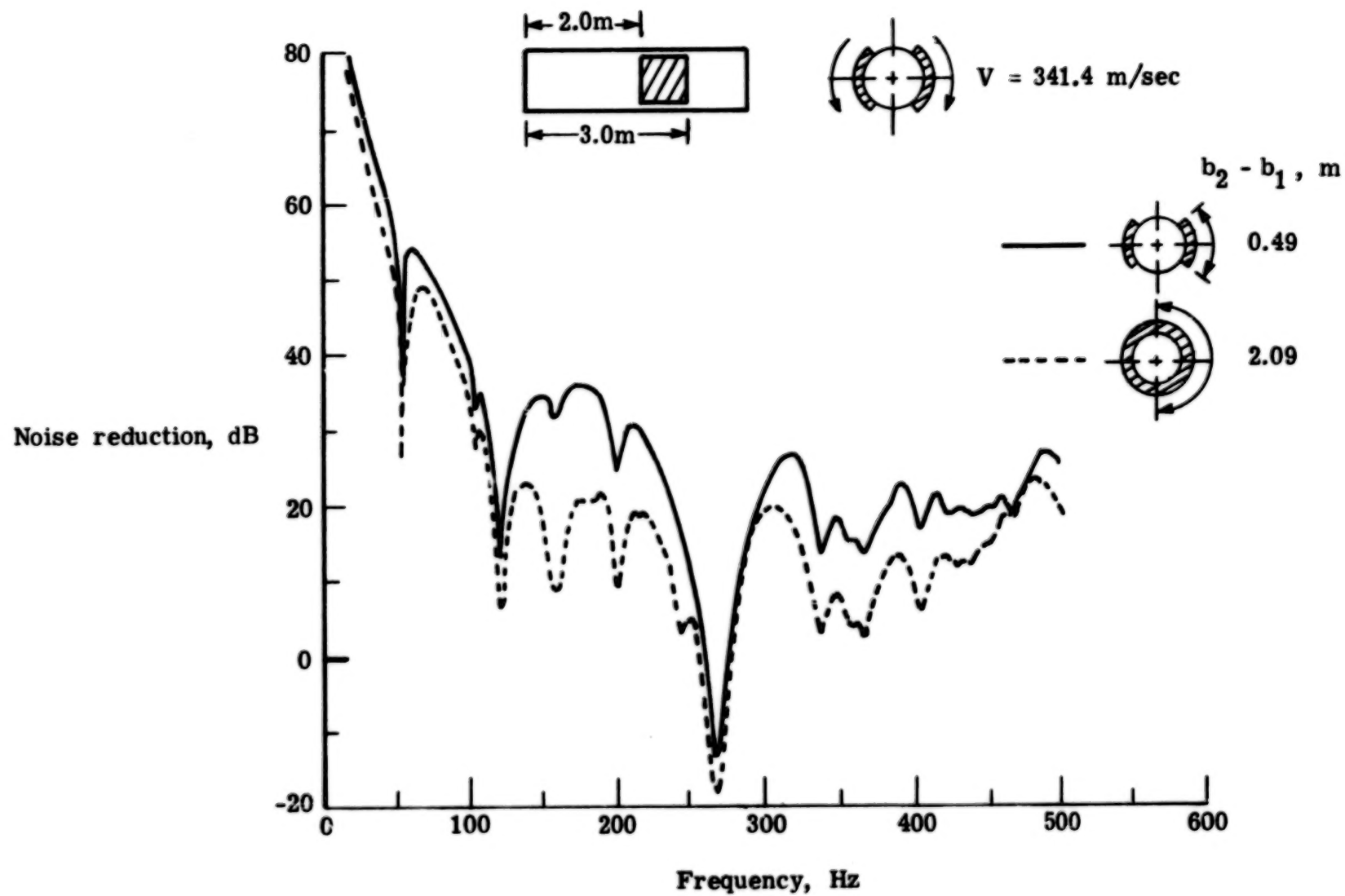exposed to noise excitation.

41

(b) Fuselage 2.

Figure 11.- Concluded.

(a) Fuselage 1.

Figure 12.- Effect on noise reduction of reducing circumferential area
exposed to noise excitation.

(b) Fuselage 2.

Figure 12.- Concluded.

44

1. Report No. NASA TP-1325	2. Government Accession No.	3. Recipient's Catalog No.
4. Title and Subtitle A THEORETICAL INVESTIGATION OF NOISE REDUCTION THROUGH THE CYLINDRICAL FUSELAGE OF A TWIN-ENGINE, PROPELLER-DRIVEN AIRCRAFT		5. Report Date December 1978
		6. Performing Organization Code
7. Author(s) Rama B. Bhat and John S. Mixson		8. Performing Organization Report No. L-12225
9. Performing Organization Name and Address NASA Langley Research Center Hampton, VA 23665		10. Work Unit No. 505-09-23-01
		11. Contract or Grant No.
12. Sponsoring Agency Name and Address National Aeronautics and Space Administration Washington, DC 20546		13. Type of Report and Period Covered Technical Paper
		14. Sponsoring Agency Code

15. Supplementary Notes

Rama B. Bhat: NRC-NASA Resident Research Associate, now at George Washington University Joint Institute for Advancement of Flight Sciences.
John S. Mixson: Langley Research Center.

16. Abstract

Interior noise in the fuselage of a twin-engine, propeller-driven aircraft with two propellers rotating in opposite directions is studied analytically. The fuselage is modeled as a stiffened cylindrical shell with simply supported ends, and the effect of stringers and frames is averaged over the shell surface. An approximate mathematical model of the propeller noise excitation is formulated which includes some of the propeller noise characteristics such as sweeping pressure waves around the sidewalls due to propeller rotation and the localized nature of the excitation with the highest levels near the propeller plane. Results are presented in the form of noise reduction, which is the difference between the levels of external and interior noise. The influence of propeller noise characteristics on the noise reduction is studied. The results indicate that the sweep velocity of the excitation around the fuselage sidewalls is critical to noise reduction.

17. Key Words (Suggested by Author(s)) Acoustics Noise reduction Interior noise Cylindrical fuselage Propeller noise	18. Distribution Statement Unclassified - Unlimited Subject Category 71
19. Security Classif. (of this report) Unclassified	20. Security Classif. (of this page) Unclassified	21. No. of Pages 44	22. Price* $4.50

NASA-Langley, 1978

45

END

MAR 2 0 1979